Supporting Information

Linker-Cluster Cooperativity in Confinement of Proline-Functionalized Zr-Based Metal-Organic Frameworks and its Effect on the Organocatalytic Aldol Reaction

Zarfishan Dilruba,[+a] Ardeshir D. Yeganeh,[+b] Sofia Kolin,[c] Sadia Noor,[a] Hassan Shatla, [b] Carl Wieland,[a] Bo-Hung Yu, [a] Katrin Gugeler,[d] Anna Zens,[a] Johannes Kästner, [d] Deven P. Estes,[e] Kristyna Pluhackova,[*c] Simon Krause,[*b] and Sabine Laschat[*a]

[a] Z. Dilruba, Dr. S. Noor, C. Wieland, B.-H. Yu, Dr. A. Zens, Prof. S. Laschat
Institut für Organische Chemie, Universität Stuttgart,
Pfaffenwaldring 55, D-70569 Stuttgart (Germany)
E-mail: sabine.laschat@oc.uni-stuttgart.de

[b] A. D. Yeganeh H. Shatla, Dr. S. Krause
Nanochemistry Department
Max Planck Institute for Solid State Research
Heisenbergstr. 1, D-70569 Stuttgart (Germany)
E-mail: s.krause@fkf.mpg.de

[c] S. Kolin, Dr. K. Pluhackova
Stuttgart Center for Simulation Science (SC SimTech),
Cluster of Excellence EXC 2075 SimTech, Universität Stuttgart,
Universitätsstr. 32, D-70569 Stuttgart (Germany)
E-mail: kristyna.pluhackova@simtech.uni-stuttgart.de

[d] K. Gugeler, Prof. Dr. J. Kästner
Institut für Theoretische Chemie, Universität Stuttgart,
Pfaffenwaldring 55, D-70569 Stuttgart (Germany)

[e] Prof. Dr. D. P. Estes
Institut für Technische Chemie, Universität Stuttgart,
Pfaffenwaldring 55, D-70569 Stuttgart (Germany)

[+] These coauthors contributed equally to this work

Table of Contents

1. Materials and Methods

1.1. General experimental Methods

Chemicals and solvents were used as received from the supplier unless stated otherwise. Anhydrous solvents were obtained by distillation under a nitrogen atmosphere using suitable drying agents. Ethyl acetate and hexanes were distilled prior to their use as eluents in column chromatography. Solvents for catalysis were degassed with nitrogen. All NMR spectra were recorded on a Bruker Avance 300 (^{1}H, 300 MHz; ^{13}C, 75 MHz), Avance 400 (^{1}H, 400 MHz; ^{13}C, 101 MHz), Avance 500 (^{1}H, 500 MHz; ^{13}C, 126 MHz) or an Avance 700 (^{1}H, 700 MHz; ^{13}C, 176 MHz) spectrometer at room temperature. The NMR spectra were referenced to tetramethylsilane (δ = 0.00 ppm) and calibrated on the respective residual solvent peaks. Infrared spectra were recorded on a Bruker Vektor22 spectrometer equipped with an MKII golden gate single reflection diamond ATR system. All mass spectra were recorded with a Bruker Daltonics micro-TOF-Q using electrospray ionization (ESI) with nitrogen as carrier gas. Specific rotation values $[a]_D^{20}$ were determined with a Perkin Elmer Polarimeter 241 at 20 °C using the sodium D-line (λ = 589 nm). All HPLC chromatograms were recorded on a Shimadzu LC-20AT setup consisting of a LC-20A pump, a DGU-20A5 degasser, a SIL-20A autosampler and an SPD-20A UV-Vis detector operating at λ = 254 nm. For the mobile phase *n*-hexane/isopropanol mixtures were used. The stationary phase was a chiral AD-H column. The chromatograms were evaluated with the program LCsolution v.1.21 from LabSolutions.
Zirconium dichloride oxide octahydrate ($ZrOCl_2.8H_2O$) was purchased from Alfa Aesar. 4,4'-Biphenyldicarboxylic acid (H4BPDC) was obtained from TCI. *N,N*-dimethylformamide (DMF) and glacial acetic acid were purchased from VWR Chemicals. Methanol was purchased from Carl Roth. Trifluoroacetic Acid (TFA) was purchased from Thermo Scientific.

Ultrasonication was conducted via VWR ultrasonic cleaning bath with 45 kHz transducer. Centrifugation was carried out with a benchtop centrifuge Sigma-3-30K from SIGMA.

Supercritical CO_2 ($scCO_2$) rinsing and drying were performed with a Leica EM CPD300 critical point dryer. The sample container was initially half-filled with MeOH at 13 °C. After CO_2 infusion, the fluid was stirred for 15 min. The exchange cycle was conducted 20 times. CO_2 was removed at 40 °C.

Powder X-ray Diffraction (PXRD): PXRD patterns were collected on a Stoe Stadi-P diffractometer in Debye-Scherrer geometry with Co-Kα1 radiation (λ = 1.78896 Å), a Ge(111) Johann monochromator, and a DECTRIS Mythen 1K detector. The samples were loaded into 0.5 mm inner diameter glass capillaries which were spun during the measurement and

analysed over a range of 2θ = 2–56˚ with 0.015˚ step size. Simulated PXRD patterns were calculated from the crystallographic information files using Mercury software.

Nitrogen Physisorption analysis: Nitrogen sorption measurements were executed using a Quantachrome Instruments Autosorb iQ 3 with N_2 at 77 K. Before the sorption analysis, the samples underwent activation under vacuum conditions at 120 °C for a duration of 12 h. The entire process was facilitated through the ASiQwin software version 3.01.

Scanning Electron Microscopy (SEM): SEM images were acquired using a Merlin Zeiss Scanning Electron Microscope with a secondary electron detector in combination with an accelerating voltage of 1.5 kV.

NMR Spectroscopy and MOF digestion: The JEOL ECZ 400S 400 MHz spectrometer was used to acquire ^{1}H-NMR spectra of the digested MOF samples. 5 mg of each MOF samples were placed into an NMR tube, followed by the addition of 600 µL of a 1M NaOH in D_2O solution, the tube was inverted 2-3 times before incubation for 24 h. This process ensures the dissolution of the organic part of the MOF, while the inorganic portion precipitates at the bottom of the tube as ZrO_2, which does not interfere with the spectra.

Thermogravimetric analysis (TGA) was recorded on a Netzsch STA 449F3 thermal analyser with Al_2O_3 crucibles under synthetic air (gas flow of 70 ml/min) with the heating rate of 5 °C/min.

2. Synthesis of proline-functionalized linkers and soluble organocatalysts

2.1. Synthesis of N-Boc-proline functionalized linkers

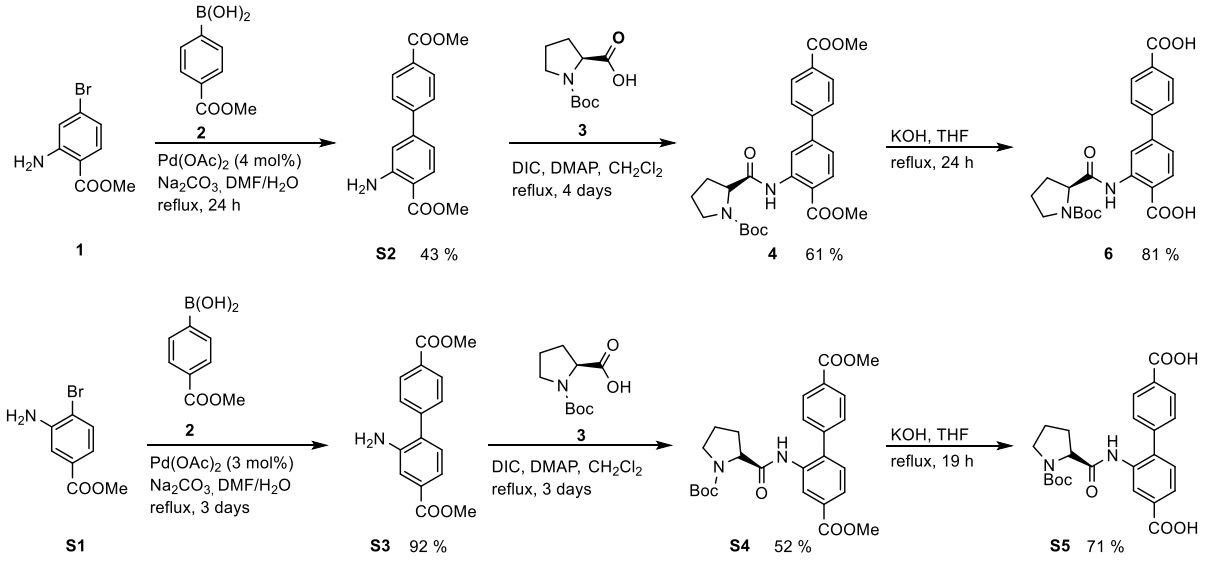

Scheme S1. Synthesis of *N*-Boc-proline functionalized *ortho*- and *meta*-diphenyl linkers.

Dimethyl-3-amino-[1,1'-biphenyl]-4,4'-dicarboxylate (S2)

Under a nitrogen atmosphere, methyl 2-amino-4-bromobenzoate **1** (5.00 g, 21.73 mmol), 4-(methoxycarbonylphenyl)boronic acid **2** (8.00 g, 44.45 mmol), palladium(II) acetate (0.13 g, 0.58 mmol) and sodium carbonate (11.00 g, 103.78 mmol) were dissolved in degassed *N*,*N*-dimethylformamide (40 mL) and degassed H_2O (40 mL). The reaction mixture was refluxed for 24 h. It was then cooled to room temperature and H_2O (300 mL) was added to the solution. The green powder **S2** (2.64 g, 9.25 mmol, 43%) was collected by filtration.

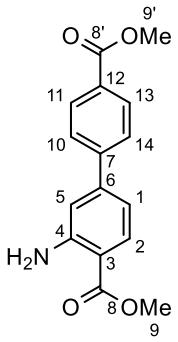

$C_{16}H_{15}NO_4$
285.30 g/mol

S2

^{1}H NMR (400 MHz, $CDCl_3$): δ = 3.89 (s, 3H, H-9), 3.94 (s, 3H, H-9'), 5.83 (s, 2H, NH_2), 6.89 (m, 2H, 1-H, 5-H), 7.63 (d, *J* = 8.3 Hz, 2H, 10-H, 14-H), 7.93 (d, *J* = 8.8 Hz, 1H, 2-H), 8.10 (d, *J* = 8.7 Hz, 2H, 11-H, 13-H) ppm. ^{13}C NMR (101 MHz, $CDCl_3$): δ = 51.8 (C-9), 52.3 (C-9'), 110.5 (C-3), 115.2 (C-5), 115.6 (C-1), 127.2 (C-14, C-10), 129.8 (C-12), 130.2 (C-11, C-13), 132.1 (C-2), 144.8 (C-7), 145.6 (C-6), 150.8 (C-4), 167.0 (C-8'), 168.5 (C-8) ppm. FTIR (ATR): $\tilde{\nu}$ = 3502 (w), 3470 (w), 3388 (w), 3368 (w), 3103 (w), 2948 (w), 2921 (vs), 1748 (w), 1718 (m), 1711 (m), 1707 (m), 1697 (w), 1683 (s), 1634 (w), 1620 (m), 1611 (m), 1591 (m), 1573 (m), 1558 (w), 1548 (w), 1477 (w), 1432 (m), 1410 (w), 1397 (w), 1340 (w), 1314 (m), 1308 (w), 1293 (m), 1265 (m), 1252 (s), 1242 (m), 1234 (s), 1208 (w), 1193 (m), 1177 (w), 1169 (m), 1136 (w), 1108 (s), 1099 (m), 1091 (s), 1040 (w), 1016 (w), 983 (w), 967 (w), 924 (w), 908 (w), 883 (w), 857 (m), 840 (w), 822 (w), 779 (w), 761 (s), 745 (w), 730 (w), 716 (w), 702 (m), 679 (w), 671 (w), 592 (w), 553 (w), 461 (w), 451 (w), 437 (w), 416 (w) cm^{-1}. HRMS (ESI): *m*/*z* = 286.1 $[M + H]^+$, 308.1 $[M + Na]^+$.

Dimethyl-(*S*)-3-(1-(tert-butoxycarbonyl)pyrrolidine-2-carboxamido)-[1,1'-biphenyl]-4,4'-dicarboxylate (4)

To a solution of *N*-Boc-L-proline **3** (5.60 g, 26.30 mmol) and DMAP (0.08 g, 0.68 mmol) in CH_2Cl_2 (40 mL), *N*,*N'*-diisopropylcarbodiimide (2.00 mL, 12.8 mmol) was added dropwise at 0 °C over 1 h. To the resulting suspension a solution of amine **S2** (2.44 g, 8.55 mmol) in CH_2Cl_2 (20 mL) was gradually added at 0 °C. The resulting mixture was then refluxed for 19 h. The organic layer was washed with H_2O (70 mL), 1 M HCl (10 mL), sat. NaCl solution (2 x 50 mL) and the combined organic layers were dried over $MgSO_4$. The solvent was

removed under reduced pressure. The crude product was purified by column chromatography on silica (hexanes / EtOAc = 4 : 1) and **4** was obtained as a colourless oil (2.50 g, 5.18 mmol, 61%).

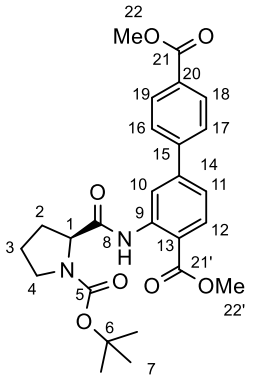

$C_{26}H_{30}N_2O_7$
482.53 g/mol

4

^{1}H NMR (400 MHz, $CDCl_3$): δ = 1.42 (d, *J* = 76.3 Hz, 9H, 7-H), 1.84 – 2.02 (m, 2H, 3-H), 2.07 – 2.38 (m, 2H, 2-H), 3.33 – 3.77 (m, 1H, 4-H), 3.55 – 3.68 (m, 1H, 4-H), 3.91 (s, 6H, 22-H, 22'-H, CO2Me), 4.22 – 4.51 (m, 1H, 1-H), 7.33 (dd, *J* = 8.4, 20.1 Hz, 1H, 11-H), 7.73 (d, *J* = 7.9 Hz, 2H, 16-H, 17-H), 8.09 (s, 3H, H-12, H-18, H-19), 9.13 (d, *J* = 12.4 Hz, 1H, H-10), 11.57 (d, *J* = 25.4 Hz, NH) ppm.^{13}C NMR (126 MHz, $CDCl_3$): δ = 23.9, 24.5 (C-3), 28.3, 28.5 (C-7), 30.6, 31.7 (C-2), 46.9, 47.3 (C-4), 52.3, 52.7 (C-22, C-22'), 62.2, 62.8 (C-1), 80.3, 80.4 (C-6), 114.7 (C-13), 118.7, 119.0 (C-10), 121.3, 121.5 (C-11), 127.5 (C-16, C-17), 129.87, 129.98 (C-20), 130.2 (C-18, C-19), 131.4, 131.7 (C-12), 141.5, 141.7 (C-9), 144.0, 144.1 (C-15), 145.8, 145.9 (C-14), 154.3, 155.2 (C-5), 166.9 (C-21), 168.1 (C-21'), 172.8 (C-8) ppm. FTIR (ATR): $\tilde{\nu}$ = 3264 (w), 2976 (w), 2250 (w), 1687 (vs), 1609 (m), 1581 (s), 1563 (s), 1530 (m), 1505 (s), 1434 (s), 1381 (vs), 1308 (m), 1244 (vs), 1157 (vs), 1110 (vs), 1046 (w), 1018 (m), 953 (w), 914 (s), 861 (m), 824 (m), 789 (m), 767 (vs), 728 (vs), 700 (s), 647 (m), 551 (w), 473 (w), 414 (w) cm^{-1}. LRMS (ESI): *m/z* = 483.2 $[M + H]^+$, 505.2 $[M + Na]^+$. $[\alpha]_D^{20}$ = – 57.4° [c = 10 mg/mL, CH_2Cl_2].

(*S*)-3-(1-(tert-Butoxycarbonyl)pyrrolidine-2-carboxamido)-[1,1'-biphenyl]-4,4'-dicarboxylic acid (6)

To a solution of the ester **4** (0.70 g, 4.68 mmol) was suspended in a 1 : 1 (v/v) mixture of THF and 1 M aq. KOH and the reaction mixture was refluxed for 21 h. THF was removed in *vacuo* and the remaining solution was acidified with 1 M aq. HCl to pH = 2. The white precipitate was isolated by filtration and washed with H_2O then dried to afford the product as yellow solid (0.54 g, 1.18 mmol, 81%).

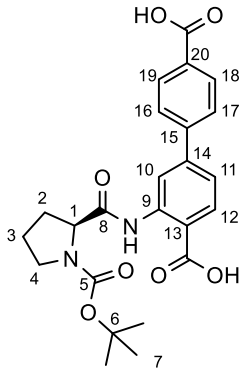

$C_{24}H_{26}N_2O_7$
454.48 g/mol

6

^{1}H NMR (400 MHz, DMSO-*d*6): δ = 1.32 (d, *J* = 66.0 Hz, 9H, 7-H), 1.81 – 1.90 (m, 2H, 3-H), 1.95 – 2.02 (m, 1H, 3-H), 2.17 – 2.34 (m, 1H, 2-H), 3.37 – 3.48 (m, 1H, 4-H), 3.48 – 3.58 (m, 1H, 4-H), 4.14 – 4.24 (m, 1H, 1-H), 7.51 (d, *J* = 6.7 Hz, 1H, 11-H), 7.80 (d, *J* = 8.2 Hz, 2H, 16-H, 17-H), 8.04 – 8.13 (m, 3H, H-12, H-18, H-19), 9.08 (d, *J* = 6.7 Hz, 1H, H-10), 11.80 (s, 1H, NH) ppm. ^{13}C NMR (101 MHz, DMSO-*d*6) = δ 23.3 (C-3), 27.9 (C-7), 31.0 (C-2), 46.5 (C-4), 62.2 (C-1), 79.0 (C-6), 115.4 (C-10), 117.3 (C-13), 121.2 (C-11), 127.1 (C-16, C-17), 130.1 (C-19, C-18), 130.7 (C-20), 132.0 (C-12), 141.3 (C-9), 143.0 (C-15), 144.5 (C-14), 154.1 (C-5), 167.0 (CO_2H), 169.5 (CO_2H), 172.2 (C-8) ppm. FTIR (ATR): $\tilde{\nu}$ = 2970 (w), 2013 (w), 1673 (m), 1607 (w), 1583 (w), 1563 (w), 1507 (w), 1395 (w), 1293 (w), 1259 (w), 1159 (w), 1122 (w), 926 (w), 804 (w), 765 (w), 665 (w), 539 (w) cm^{-1}. LRMS (ESI): *m*/*z* = 455.2 [M + H]$^+$, 477.2 [M + Na]$^+$. $[a]_D^{20}$ = – 697.8° [c = 10 mg/mL, DMSO].

Dimethyl-2-amino-[1,1'-biphenyl]-4,4'-dicarboxylate (S3)

Under a nitrogen atmosphere, methyl 3-amino-4-bromo-benzoate **S1** (5.00 g, 21.73 mmol), 4-methoxy carbonylphenylboronic acid **2** (5.87 g, 32.60 mmol), palladium(II) acetate (0.24 g, 1.09 mmol) and sodium carbonate (9.21 g, 86.9 mmol) were added to a mixed solution of deoxygenated *N*,*N*-dimethylformamide (40 mL) and H_2O (40 mL). The reaction mixture was refluxed for 19 h. It was then and cooled to room temperature and water (300 mL) was added to the solution. The green powder **S3** (5.71 g, 19.98 mmol, 92%) was collected by filtration.

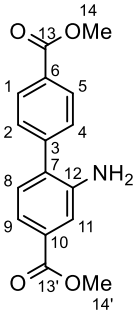

$C_{16}H_{15}NO_4$
285.30 g/mol

S3

^{1}H NMR (400 MHz, $CDCl_3$): δ = 3.87 (s, 2H, NH_2), 3.91 (s, 3H, 14-H), 3.96 (s, 3H, 14-H'), 7.17 (d, *J* = 7.88 Hz, 1H, H-11), 7.41 – 7.52 (m, 2H, H-2, H-4), 7.53 – 7.58 (m, 2H, H-8. H-9), 8.13

(d, *J* = 8.51 Hz, 2H, H-1, H-5) ppm. ^{13}C NMR (101 MHz, $CDCl_3$): δ = 52.3 (C-14), 52.4 (C-14'), 116.8 (C-11), 127.4 (C-9), 129.0 (C-4, C-2), 129.6 (C-8), 130.4 (C-5, C-6), 130.5 (C-1), 130.6 (C-7), 130.9 (C-10), 143.5 (C-3), 143.7 (C-12), 166.9 (C-13'), 167.2 (C-13) ppm.
The spectroscopic data are in accordance with literature.[21]

Dimethyl-(*S*)-2-(1-(tert-Butoxycarbonyl)pyrrolidine-2-carboxamido)-[1,1'-biphenyl]-4,4'-dicarboxylate (S4)

To a solution of *N*-Boc-L-proline **3** (656 mg, 2.3 mmol) and DMAP (15 mg, 0.12 mmol) in CH_2Cl_2 (20 mL), *N*,*N'*-diisopropylcarbodiimide (3.60 mL, 2.3 mmol) was added dropwise at 0 °C over 1 h. To the resulting suspension a solution of **S3** (0.440 g, 1.54 mmol) in CH_2Cl_2 (20 mL) was gradually added at 0 °C. The resulting mixture was then refluxed for 48 h. The organic layer was washed with H_2O (20 mL) and sat. NaCl solution (50 mL) and the combined organic layers were dried over $MgSO_4$. The solvent was removed under reduced pressure. The crude product was purified by column chromatography on silica (hexanes / EtOAc = 2 : 1). Product **S4** was obtained as a white solid (0.39 g, 0.81 mmol, 52%). [21]

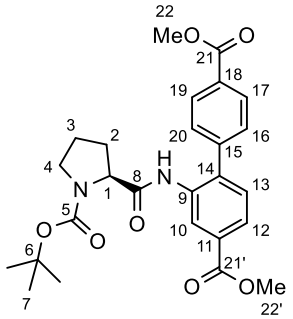

$C_{26}H_{30}N_2O_7$
482.53 g/mol

S4

^{1}H NMR (300 MHz, $CDCl_3$, complicated by conformers): δ = 1.33 (s, 9H, 7-H), 1.76 – 2.49 (m, 4H, 3-H, 2-H), 3.18 (d, *J* = 41.9 Hz, 2H, 4-H), 3.94 (d, *J* = 6.0 Hz, 6H, 22-H, 22'-H), 4.24 (s, 1H, 1-H), 7.32 (d, *J* = 8.0 Hz, 1H, C-13), 7.43 (d, *J* = 8.1 Hz, 2H, H-16, H-20), 7.88 (dd, *J* = 1.8, 8.0 Hz, 1H, H-12), 8.15 (dd, *J* = 1.9, 8.3 Hz, 2H, H-17, H-19), 8.92 (s, 1H, H-10) ppm. ^{13}C NMR (101 MHz, $CDCl_3$, complicated by conformers) δ = 23.3 (C-3), 24.4 (C-3), 28.3 (C-7), 28.5 (C-7), 31.0 (C-2), 47.2 (C-4), 52.4 (C-22), 59.3 (C-1), 80.9 (C-6), 81.7 (C-6), 125.9 (C-12), 129.1 (C-17, C-19), 130.1 (H-16. H-20), 130.4 (C-13), 166.7 (C-21, C-22') ppm.
The spectroscopic data are in accordance with literature.[22]

(*S*)-2-(1-(tert-butoxycarbonyl)pyrrolidine-2-carboxamido)-[1,1'-biphenyl]-4,4'-dicarboxylic acid (S5)

N-Boc-protected dimethylester **S4** (1.40 g, 2.90 mmol) was suspended in a 1 : 1 (v/v) mixture of THF and 1 M aq. KOH (10 mL) and was refluxed for 19 h. THF was removed in *vacuo*. The remaining solution was acidified with 1 M aq. HCl to pH = 2. The white precipitate was isolated

by filtration and washed with H_2O then dried to afford the product **S5** as an off-white solid (0.94 g, 2.07 mmol, 71%).[21]

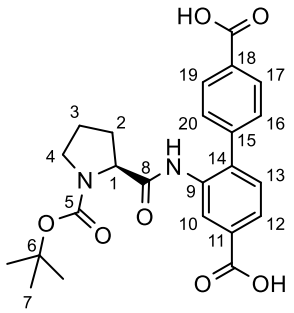

$C_{24}H_{26}N_2O_7$
454.48 g/mol

S5

^{1}H NMR (700 MHz, D_2O/KOH): δ = 1.27 – 1.35 (m, 1H, H-3), 1.34 – 1.39 (s, 9H, H-7), 1.46 – 1.56 (m, 1H, H-3), 1.70 (dp, *J* = 6.5, 12.8 Hz, 1H), H-4, 2.01 (dq, *J* = 8.0, 12.8 Hz, 1H, H-4), 3.25 – 3.32 (m, 2H, H-2), 4.14 (dd, *J* = 5.0, 8.6 Hz, 1H, H-1), 7.37 (d, *J* = 7.9 Hz, 2H, 20-H, 16-H), 7.44 (dd, *J* = 4.5, 8.2 Hz, 1H, H-13), 7.79 (d, *J* = 1.7 Hz, 1H, H-12), 7.86 (dd, *J* = 1.8, 8.0 Hz, 1H, H-10), 7.93 (dd, *J* = 2.7, 9.4 Hz, 2H, 17-H, 19-H) ppm. ^{13}C NMR (126 MHz, DMSO-d*6*) δ = 23.1 (C-3), 23.9 (C-3), 28.1 (C-7), 29.5 (C-2), 30.5 (C-2), 46.5 (C-4), 46.8 (C-4), 60.0 (C-1), 78.6 (C-6), 117.5 (C-10), 126.7 (C-12), 127.2 (C-16, C-20), 128.9 (C-13), 130.1 (C-17, C-19), 130.5 (C-11), 130.9 (C-18), 135.0 (C-14), 138.9 (C-9), 143.1 (C-15), 153.8 (C-5), 167.2 (CO_2H), 167.2 (CO_2H), 171.5 (C-8) ppm.

The spectroscopic data are in accordance with literature.[23]

2.2. Synthesis of soluble catalysts

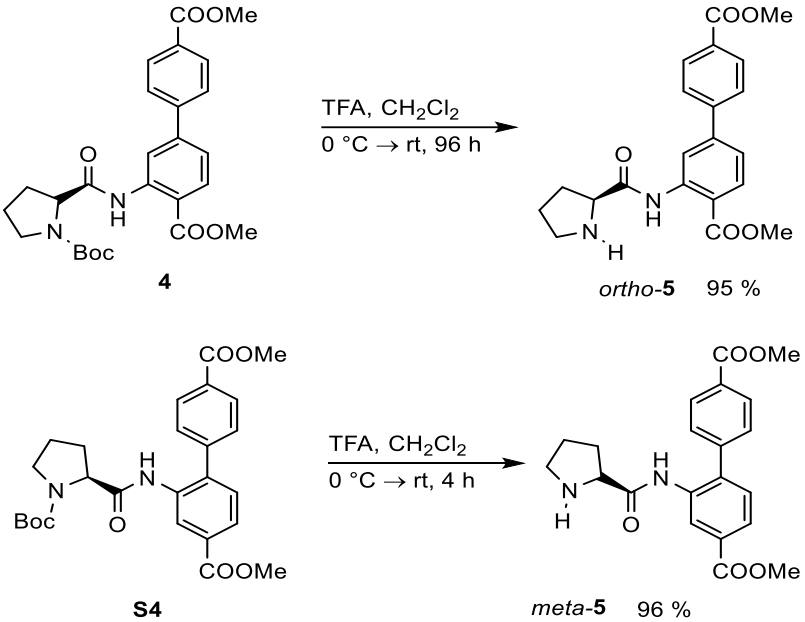

Scheme S2: Synthesis of soluble *ortho*- and *meta*-biphenyl catalysts.

Dimethyl-(*S*)-3-(pyrrolidine-2-carboxamido)-[1,1'-biphenyl]-4,4'-dicarboxylate (*ortho*-5)

According to ref. [21] to a solution of *N*-Boc-protected amide **4** (2.00 g, 4.02 mmol) in CH_2Cl_2 (25 mL) trifluoroacetic acid (20 mL) was added dropwise at 0 °C. After 10 min, the reaction mixture was allowed to warm to room temperature and stirred for 96 h at room temperature. The reaction mixture was neutralised with sat. aq. $NaHCO_3$ (60 mL) and the aqueous layer was extracted with CH_2Cl_2 (3 × 50 mL) and washed with sat. NaCl solution (50 mL). The combined organic layers were dried over $MgSO_4$ and solvent was removed under reduced pressure. The amide *ortho*-**5** was obtained as a yellow solid (1.50 g, 3.92 mmol, 95%) without further purification.

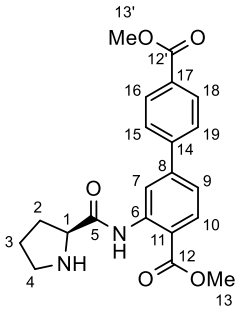

$C_{21}H_{22}N_2O_5$
382.42 g/mol

ortho-***5***

^{1}H NMR (500 MHz, $CDCl_3$): δ = 1.80 (dddd, J = 5.8, 7.3, 12.9, 20.2 Hz, 2H, 3-H), 2.08 (m, 1H, 2-H), 2.25 (ddt, J = 7.5, 8.9, 12.8 Hz, 1H, 2-H), 3.10 (dt, J = 6.5, 10.4 Hz, 1H, 4-H), 3.17 (dt, *J* = 6.8, 10.4 Hz, 1H, 4-H), 3.93 (s, 3H, H-13), 3.95 (s, 3H, H-13'), 3.96 – 4.00 (m, 1H, H-1), 7.33 (dd, *J* = 1.9, 8.3 Hz, 1H, 9-H), 7.73 (7.70 – 7.75 (d, *J* = 8.3 Hz, 2H, 15-H, 19-H), 8.06 – 8.11 (m, 3H, H-10, H-16, H-18), 9.12 – 9.15 (d, *J* = 1.8 Hz, 1H, H-7), 12.18 – 12.22 (s, 1H, N-H) ppm. ^{13}C NMR (126 MHz, $CDCl_3$): δ = 26.3 (C-3), 31.3 (C-2), 47.5 (C-4), 52.3 (C-13), 52.5 (C-13'), 62.0 (C-1), 115.5 (C-11), 119.2 (C-7), 121.3 (C-9), 127.5 (C-15, C-19), 129.9 (C-17), 130.2 (C-18, C-16), 131.7 (C-10), 141.3 (C-6), 144.2 (C-14), 145.6 (C-8), 166.9 (C-12), 167.8 (C-12'), 175.2 (C-5) ppm. FTIR (ATR): $\tilde{\nu}$ = 3853 (w), 3199 (w), 3060 (w), 2952 (w), 2030 (w), 1701 (s), 1628 (w), 1607 (m), 1593 (w), 1577 (m), 1571 (m), 1556 (s), 1542 (m), 1524 (s), 1514 (m), 1503 (s), 1481 (w), 1459 (s), 1446 (m), 1434 (s), 1408 (w), 1395 (s), 1352 (w), 1250 (vs), 1206 (m), 1189 (s), 1169 (m), 1155 (m), 1132 (w), 1093 (vs), 1059 (w), 1046 (m), 1030 (w), 1018 (m), 995 (w), 965 (w), 947 (w), 912 (m), 877 (w), 861 (m), 851 (m), 824 (m), 798 (w), 787 (m), 779 (w), 767 (vs), 751 (w), 728 (vs), 712 (m), 700 (s), 679 (w), 647 (m), 541 (w), 449 (w) cm^{-1}. LRMS (ESI): *m*/*z* = 383.2 $[M + H]^+$. $[a]_D^{20}$ = – 39.0 ° [c = 10 mg/mL, CH_2Cl_2].

Dimethyl-(*S*)-2-(pyrrolidine-2-carboxamido)-[1,1'-biphenyl]-4,4'-dicarboxylate (*meta*-5)

According to ref.[21] to a solution of *N*-Boc-protected amide **S4** (1.65 g, 4.06 mmol) in CH_2Cl_2 (10 mL) trifluoroacetic acid (10 mL) was added dropwise at 0 °C. After 10 min, the reaction mixture was allowed to warm to room temperature and stirred for 4 h at room temperature. The reaction mixture was neutralised with sat. aq. $NaHCO_3$ (60 mL) and the aqueous layer was extracted with CH_2Cl_2 (3 × 50 mL). The combined organic layers were dried over $MgSO_4$ and solvent was removed under reduced pressure. The amide *meta*-**5** was obtained as a white solid (1.20 g, 3.92 mmol, 96%) without further purification.

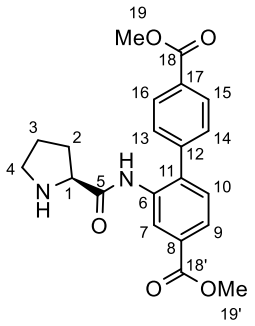

$C_{21}H_{22}N_2O_5$
382.42 g/mol

meta-**5**

^{1}H NMR (400 MHz, $CDCl_3$): δ = 1.57 – 1.87 (m, 2H, 3-H), 1.92 – 2.03 (m, 1H, 2-H), 2.07 – 2.22 (m, 1H, 2-H), 2.73 – 2.84 (m, 1H, 4-H), 2.93 – 3.04 (m, 1H, 4-H), 3.90 – 3.98 (m, 6H, 19-H, 19'-H), 4.02 (s, 1H, 1-H), 7.33 (d, *J* = 7.9 Hz, 1H, C-10), 7.41 – 7.48 (m, 2H, C-13, C-14), 7.87 (dd, *J* = 1.7, 8.0 Hz, 1H, C-9), 8.09 – 8.13 (m, 2H, 15-H, 16-H), 8.84 (s, 1H, 7-H), 9.96 (s, 1H, NH) ppm. ^{13}C NMR (101 MHz, $CDCl_3$): δ = 25.9 (C-3), 30.7 (C-2), 47.1 (C-4), 52.4 (C-19), 52.5 (C-19'), 60.8 (C-1), 123.3 (C-7), 126.0 (C-9), 127.4 (C-9), 129.3 – 130.9 (C-10, C-8, C-17, C-13, C-14, C-15, C-16), 134.9 (C-11), 142.6 (C-6, C-12), 166.7 (C-18), 166.9 (C-18') ppm.
The spectroscopic data are in accordance with literature.[22]

3. Synthesis of MOF catalysts

o-UiO-67-NH-Pro-mod

$ZrOCl_2 \cdot 8H_2O$ (0.65 mmol) was introduced into a 100 mL Schott bottle (crafted from DURAN borosilicate glass) equipped with a PTFE-coated silicone-sealed screw cap. Following this, 25 mL DMF and 995 µL of TFA (20 equiv., 0.5 mM) were added, and the mixture was sonicated until a clear solution was achieved. Subsequently, the N-Boc-proline functionalized linker (**6**) was introduced (0.65 mmol), followed by sonication. The resulting solution was placed in a pre-heated oven at 120 °C for 24 h. The resulting crystalline powder was recovered by centrifugation (4500 rpm, 10 min) and washed three times with DMF and four times with MeOH, with the last cycles conducted overnight. The product was dried with supercritical CO_2 and then under vacuum (1 x 10^{-3}) at 30 °C overnight. The synthesis of **o-UiO-67-NH-Pro** with acetic

acid (AcOH) followed a similar procedure, replacing TFA with AcOH (100 equiv., 2.26 mM), denoted as ***o*-UiO-67-NH-Pro-AcOH**. The synthesis of ***o*-UiO-67-NH-Pro** with benzoic acid (BA) was also carried out using the same procedure, changing the metal source to $ZrCl_4$ (0.65 mmol) and the modulator to BA (15 equiv., 0.39 mM), denoted as ***o*-UiO-67-NH-Pro-BA**.

***m*-UiO-67-NH-Pro-mod**

The synthesis of ***m*-UiO-67-NH-Pro-mod** with benzoic acid (BA) as the modulator was done according to the literature [15]. $ZrCl_4$ (0.39 mmol) was added to a 100 ml Schott bottle along with BA (5.85 mmol, 15 equiv.) and 15 ml DMF, and the mixture was further sonicated until a clear solution was obtained. To the resulting solution, the N-Boc-proline functionalized linker **S5** on the *meta* position was added (0.39 mmol) and sonicated briefly. The resulting solution was placed in a pre-heated oven at 120 °C for 4 d. The resulting crystalline powder was recovered by centrifugation (4500 rpm, 10 min) and washed three times with DMF and four times with MeOH, with the last cycles conducted overnight. The product was dried with supercritical CO_2 and then under vacuum (1×10^{-3}) at 30 °C overnight.

The synthesis of ***m*-UiO-67-NH-Pro-mod** with AcOH followed the exact procedure as with BA modulator, except the use of $ZrOCl_2.8H_2O$ (0.39 mmol) was used instead of $ZrCl_4$. The synthesis of ***m*-UiO-67-NH-Pro** with TFA followed a similar procedure as ***o*-UiO-67-NHPro-TFA**, except using the *meta*-functionalized linker.

UiO-67

The synthesis of **UiO-67** was done by first making a solution of $ZrOCl_2 \cdot 8H_2O$ (0.65 mmol) with 10 ml DMF and 995 µL TFA in a glass vial. Then, in a 100 ml Schott bottle, biphenyl dicarboxylic acid (H4BPDC) linker (0.65 mmol) was dissolved in 15 ml DMF with sonication and heating at 100 °C until a clear solution was obtained. After cooling down the linker solution, the zirconium solution was added, and the resulting solution was placed in the oven at 120 °C for 24h. The work up and guest removal procedure were conducted as mentioned above with proline functionalized samples.

3.1. Post-synthetic deprotection of MOF catalysts

The non-deprotected MOF samples (35-40 mg) were suspended in DMF (3 ml) in a microwave vial and heated to 180 °C for 3 h. Then the DMF was decanted and the MOFs were soaked in acetone for 3 d at room temperature, with solvent replenished daily. Finally, the samples were dried under vacuum (1×10^{-3}) at 30 °C overnight.

4. MOF characterizations

4.1. PXRD patterns

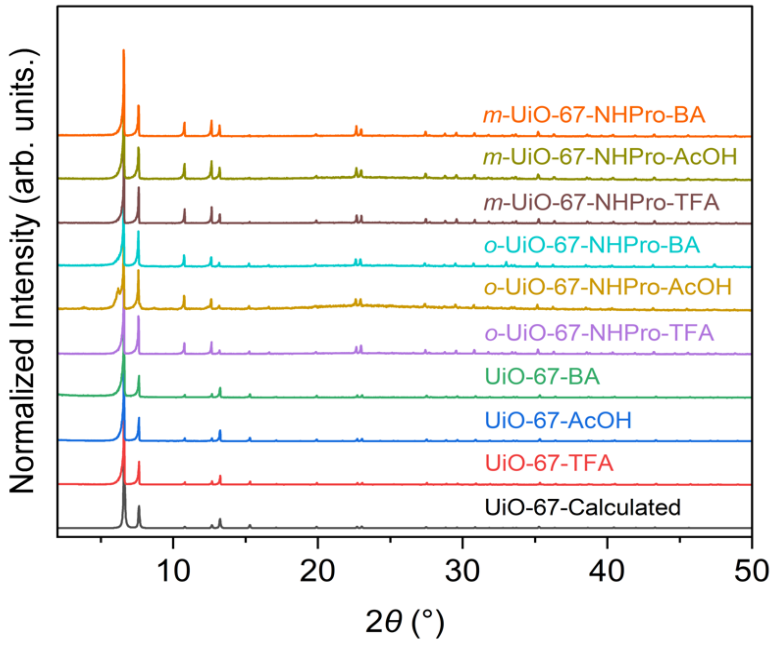

Figure S1: PXRD patterns of the as made non-functional and functionalized MOFs synthesized with TFA, AcOH and BA as modulators.

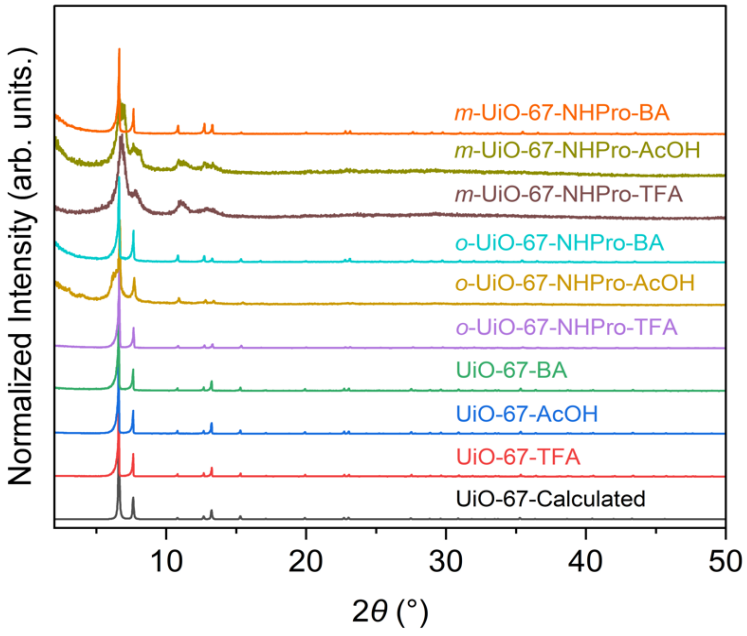

Figure S2: PXRD patterns of the activated non-functional and functionalized MOFs synthesized with TFA, AcOH and BA as modulators.

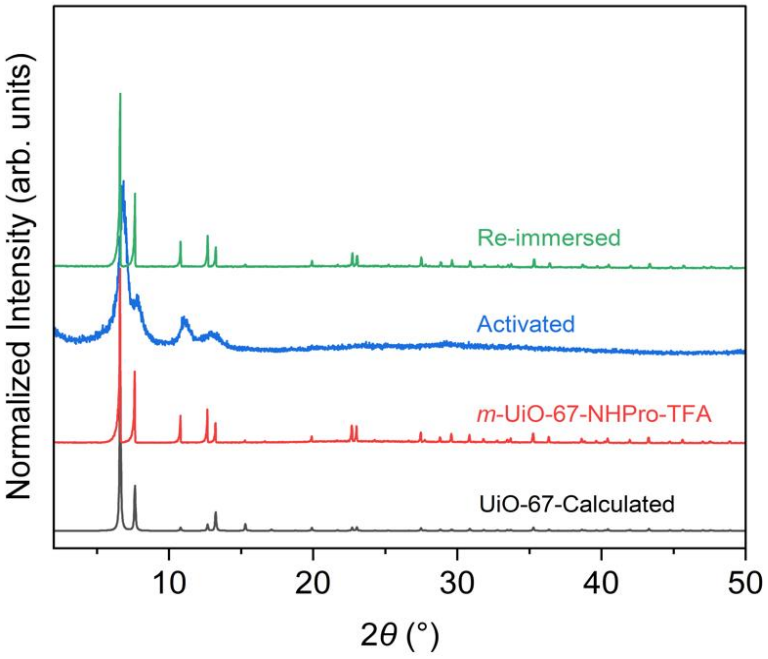

Figure S3: PXRD patterns of the as made ***m*-UiO-67-NHPro-TFA**, along with its activated patterns after drying and the re-immersed sample in solvent retaining the long-range order.

4.2. Nitrogen adsorption-desorption isotherms

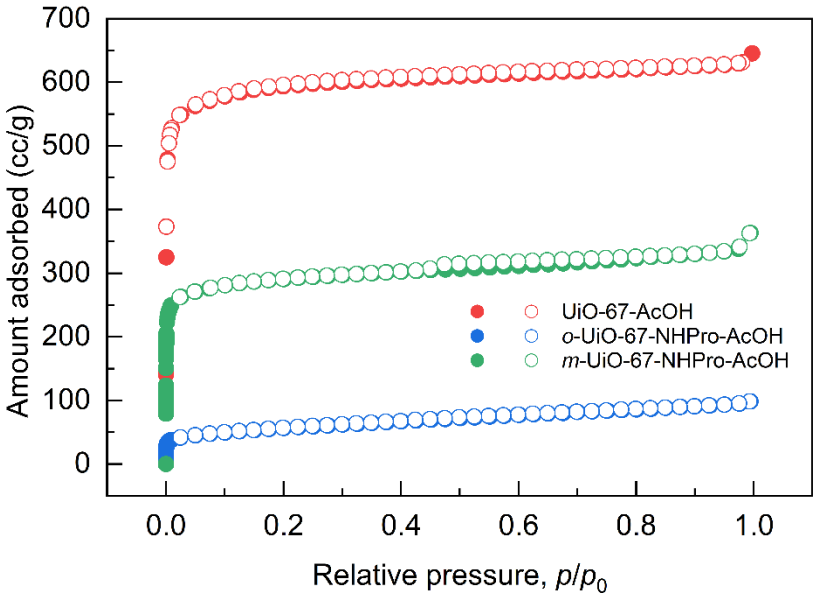

Figure S4: N_2 adsorption (filled circles) desorption (empty circles) isotherms of the AcOH modulated **UiO-67** and their respective *ortho* and *meta* proline functionalized samples.

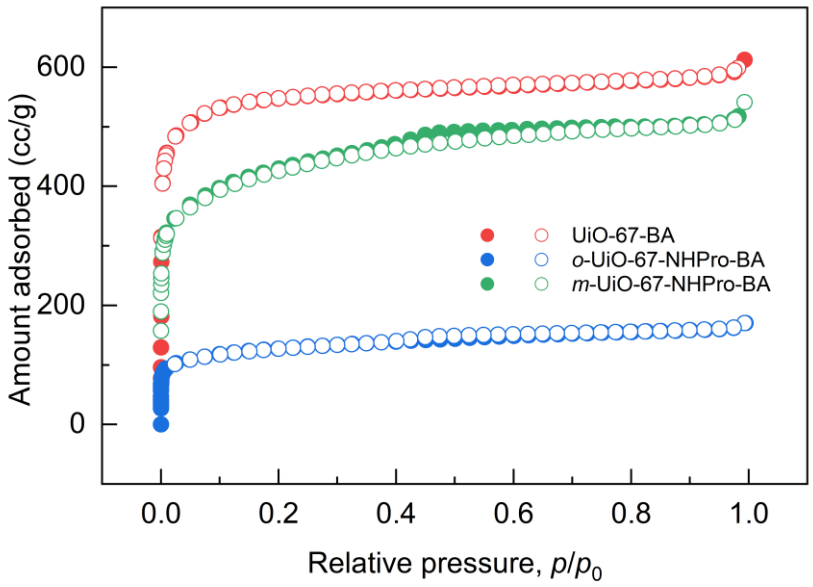

Figure S5: N_2 adsorption (filled circles) desorption (empty circles) isotherms of the BA modulated **UiO-67** and their respective *ortho* and *meta* proline functionalized samples.

4.2.1. Pore Size Distribution

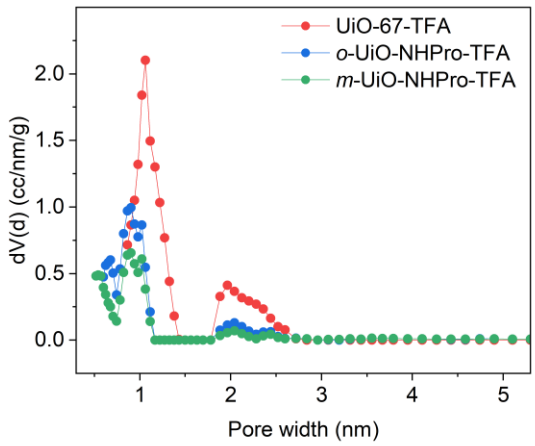

Figure S6: Pore-size Distribution of UiO-67 MOFs with TFA as modulator, determined by NLDFT, carbon cylindrical/slit pore kernel.

4.3. ^{1}H NMR spectra of digested MOF samples / modulator amounts

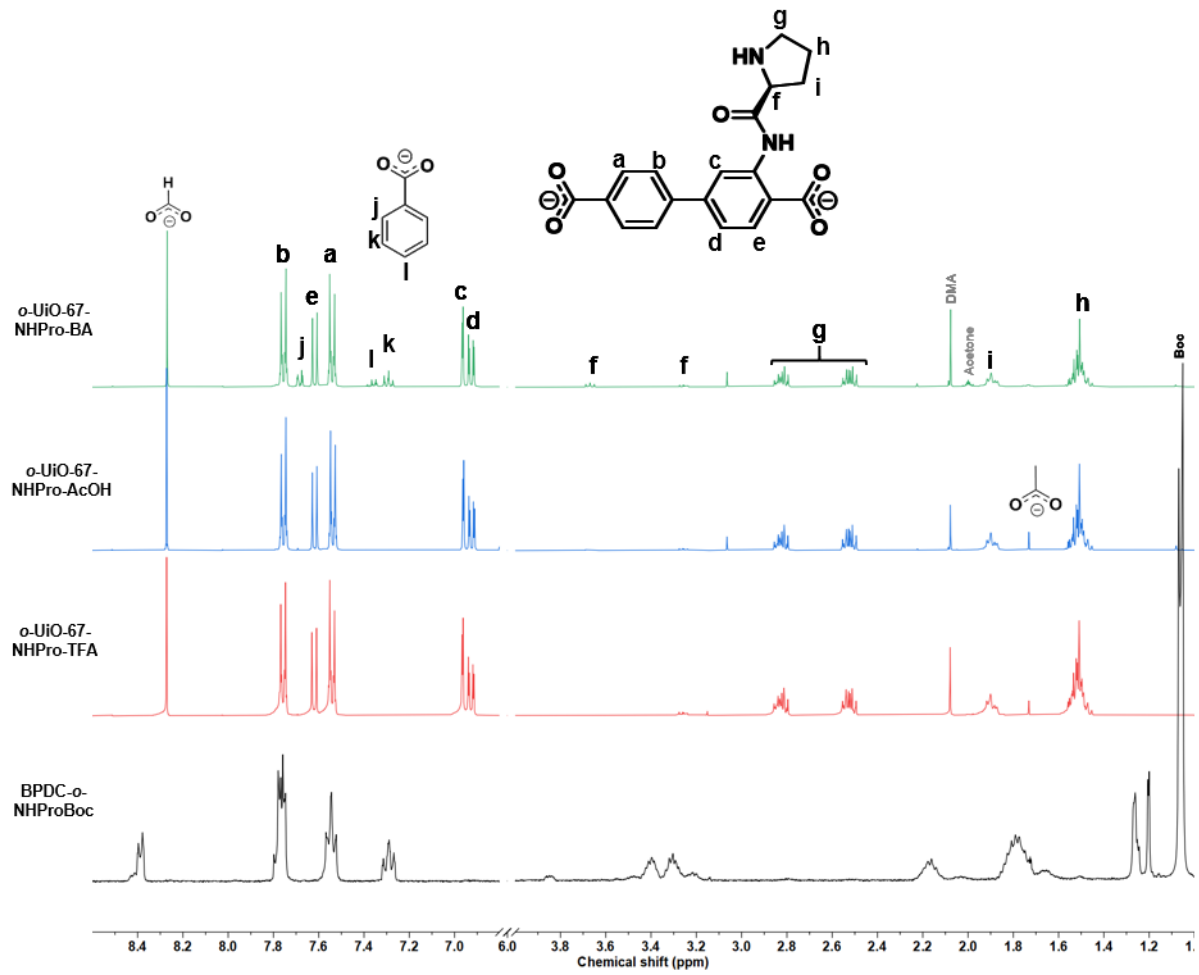

Figure S7: ^{1}H-NMR spectra of the digested *ortho* functionalized UiO-67 MOFs in 1 M solution of NaOH/D_2O.

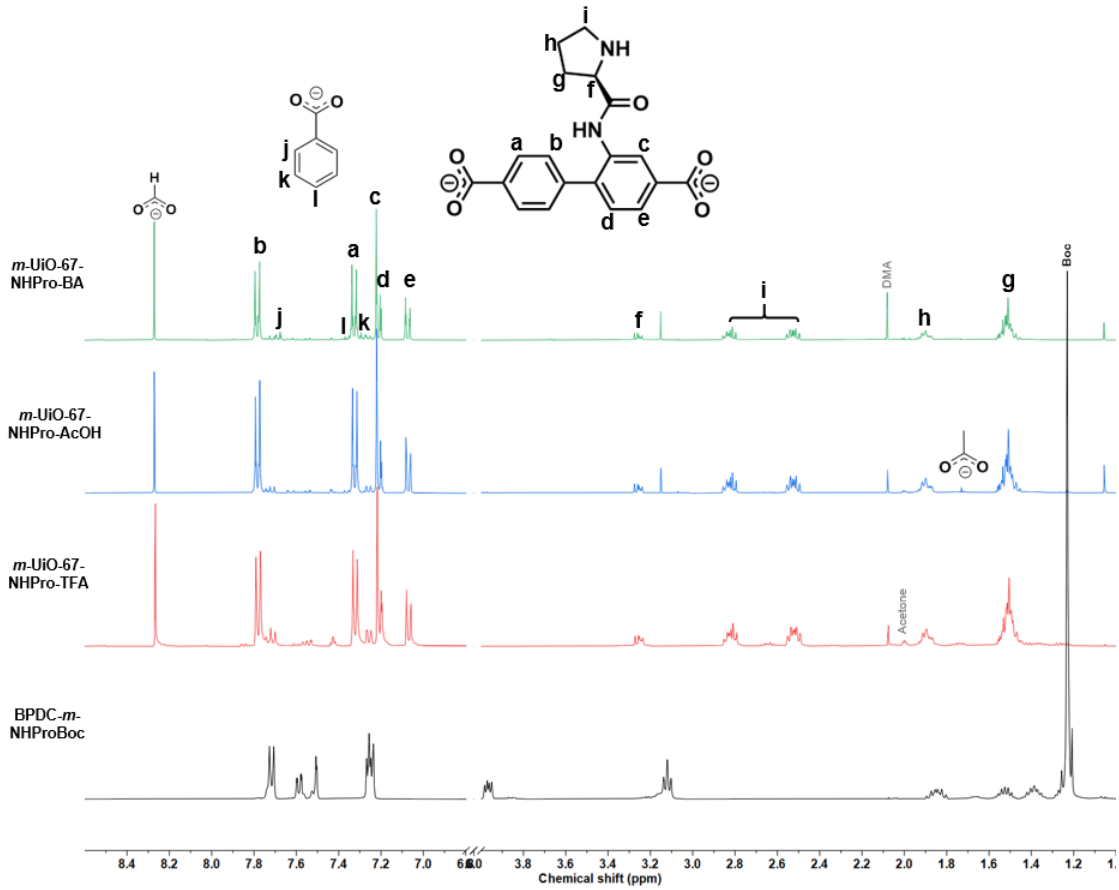

Figure S8: ^{1}H-NMR spectra of the digested *meta* functionalized UiO-67 MOFs in 1 M solution of NaOH/D_2O.

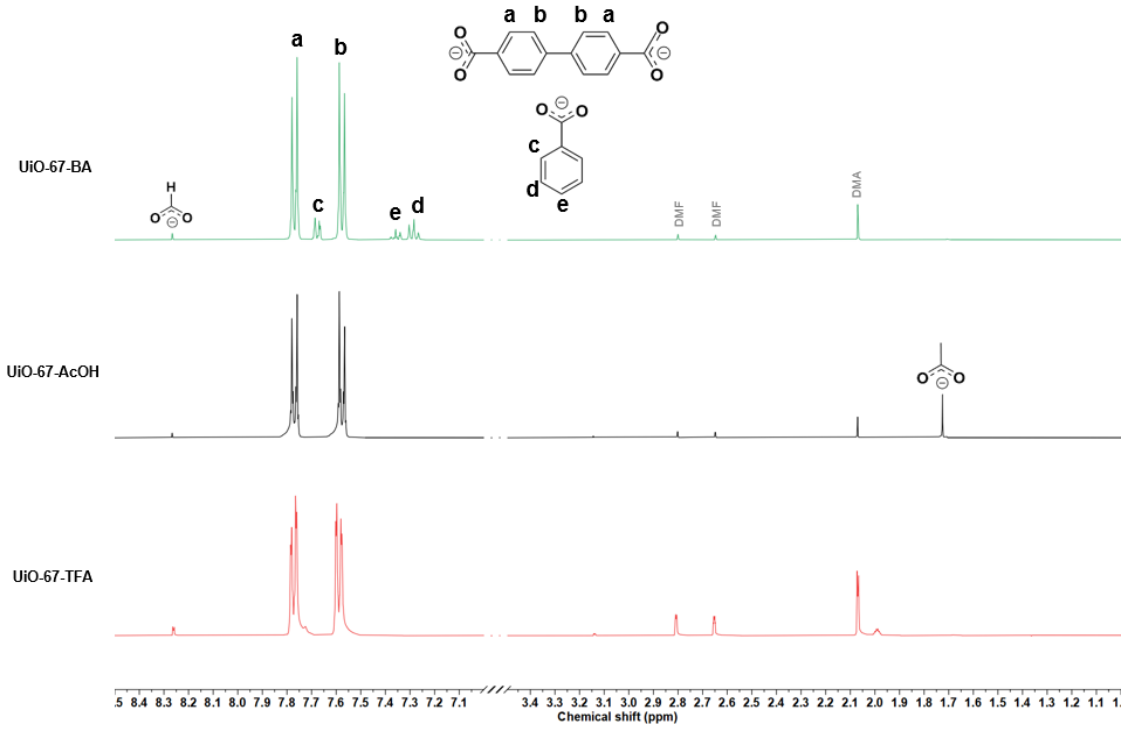

Figure S9: ^{1}H-NMR spectra of the digested UiO-67 MOFs in 1 M solution of NaOH/D_2O.

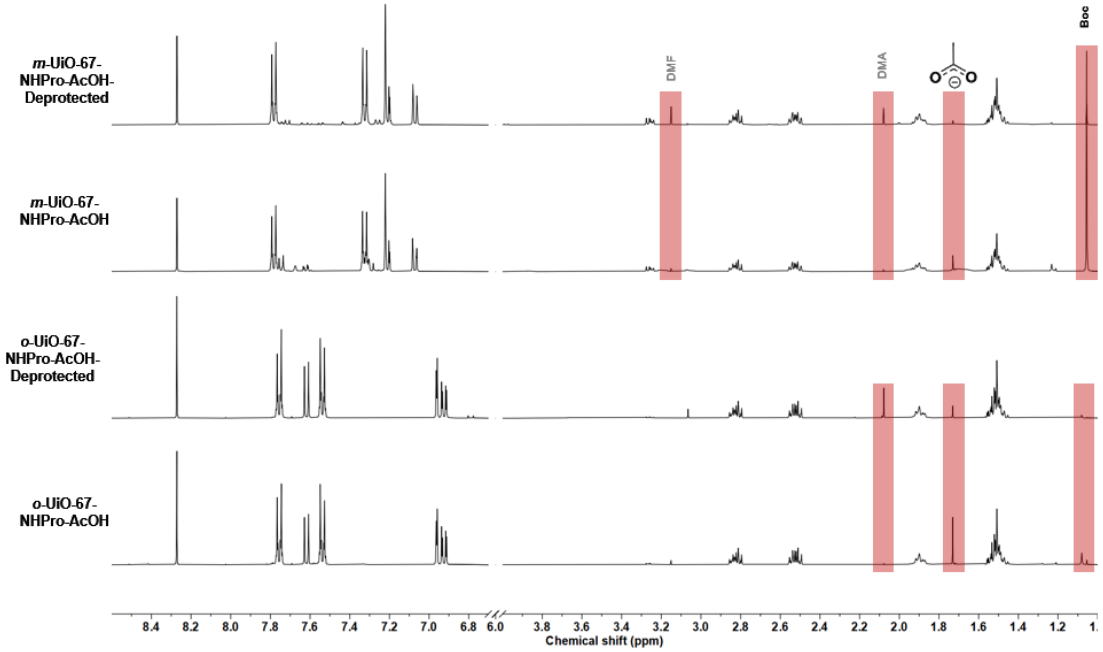

Figure S10: ^{1}H-NMR spectra of the digested UiO-67 MOFs synthesized with AcOH modulator, before and after deprotection, in 1 M solution of NaOH/D_2O.The highlighted areas are showing changes after solvothermal treatment, including Boc deprotection, decreasing the amount of modulator and increasing the amount of DMF decomposition products, eg, dimethyamine and formate.

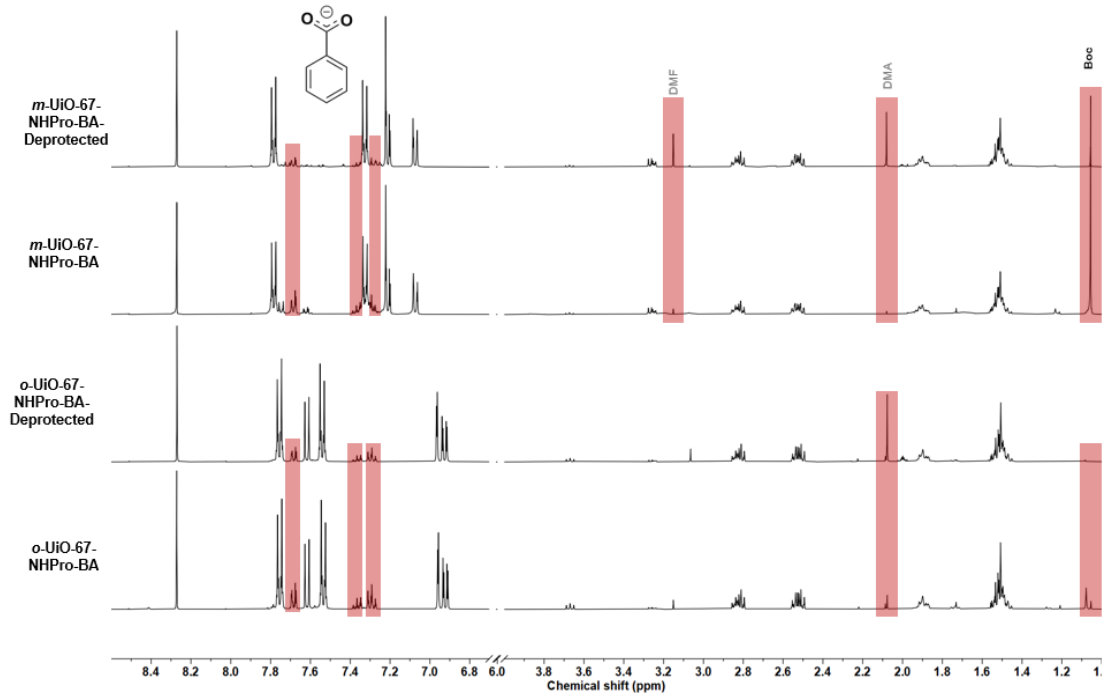

Figure S11: ^{1}H-NMR spectra of the digested UiO-67 MOFs synthesized with BA modulator, before and after deprotection, in 1 M solution of NaOH/D_2O.The highlighted areas are showing changes after solvothermal treatment, including Boc deprotection, decreasing the amount of modulator and increasing the amount of DMF decomposition products, eg, dimethylamine and formate.

.

Table S1. Modulator content in the non-functional and functionalized samples obtained from ^{1}H NMR integrals.

MOF Samples	Modulator/linker ratio[a]	Formate/linker ratio[b]
UiO-67-TFA	0.17	0.13
***o*-UiO-67-NH-Pro-TFA**	0.24	0.67
***m*-UiO-67-NH-Pro-TFA**	0.21	0.7
UiO-67-AcOH	0.08	0.02
***o*-UiO-67-NH-Pro-AcOH**	0.03	0.64
***o*-UiO-67-NH-Pro-AcOH-Depro-tected**	0.008	0.72
***m*-UiO-67-NH-Pro-AcOH**	0.02	0.65
***m*-UiO-67-NH-Pro-AcOH-Depro-tected**	0.01	0.67
UiO-67-BA	0.3	0.01
***o*-UiO-67-NH-Pro-BA**	0.25	0.53
***o*-UiO-67-NH-Pro-BA-Deprotected**	0.17	0.6
***m*-UiO-67-NH-Pro-BA**	0.34	0.67
***m*-UiO-67-NH-Pro-BA-Deprotected**	0.14	0.69

[a] mol ratio of modulators calculated by the formula: $\left(\frac{modI}{modH}\right) * \left(\frac{LinkerH}{LinkerI}\right)$ in which *I* is the integral and *H* the number of protons. Mol ratio of TFA containing samples were calculated by a combination of ^{1}H NMR and ^{19}F NMR and by using difluoro acetic acid as an internal standard.

[b] mol ratio of formate to linker also quantified with a similar as the modulator. It should be noted that the formate mol ratio could be well overestimated due to the presence of the residual amounts of DMF or DMF decomposition products in the ^{1}H NMR spectra.

4.4. Thermogravimetric Analysis (TGA)

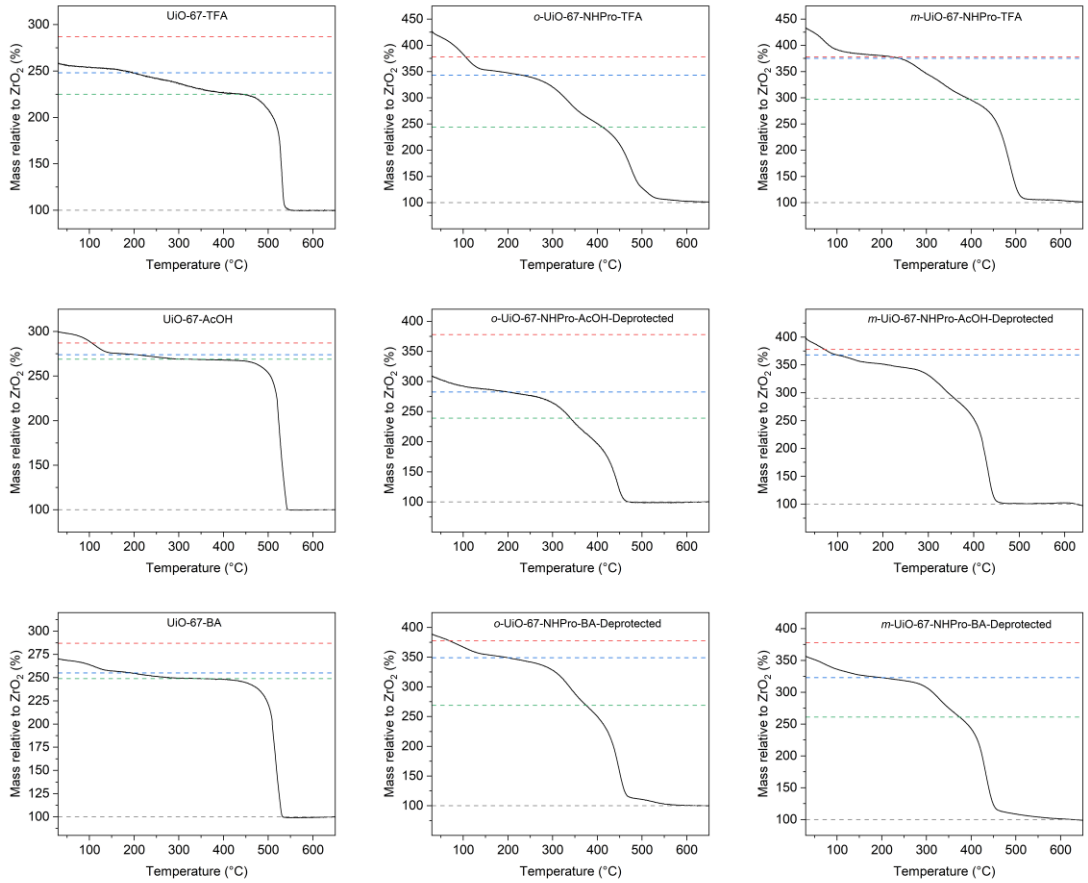

Figure S12: TGA data of MOF catalysts. The red dashed lines indicating the theoretical mass of the hydroxylated UiO MOFs and the blue dashed lines showing the mass loss at 200 °C and the dashed line showing the last step of mass loss.

We performed TGA on all the MOF systems discussed in the manuscript based on the methods described previously by Schearer *et al*. [31] and Sannes *et al.,* [32] to determine their chemical composition. These TGA data were combined with H-NMR data of the digested MOFs to derive their chemical composition based on the formula below and summarized in Table S2:

$Zr_6O_{4+2x-2y-2z}(OH)_{4-2x+2y+2z}(Linker)_{6-x}(Mod)_{2y}(Formate)_{2z}$

It is important to note that due to the mild activation conditions, residual pore contents, including solvent or solvent decomposition products (3-11% based on H-NMR of the digested MOFs), may lead to an overestimation of certain components, such as formate, in the formula. Additionally, the quantification of missing cluster defects remains uncertain, and their presence in the MOF systems studied cannot be ruled out, which could further influence the chemical composition and defect quantification calculations.

Table S2. Calculated chemical formula of the MOF catalysts used in this study, based on combination of TGA (data from the last step of mass loss) and ^{1}H-NMR modulator/linker ratio and Formate/linker ratio.

MOF Samples	Molecular formula
UiO-67-TFA	$Zr_6O_{6.72}(OH)_{1.28}(BPDC)_{4.04}(TFA)_{0.69}(Form)_{0.52}$
***o*-UiO-67-NH-Pro-TFA**	$Zr_6O_{6.95}(OH)_{1.05}(BPDC\text{-}NHPro)_{3.11}(TFA)_{0.75}(Form)_{2.08}$
***m*-UiO-67-NH-Pro-TFA**	$Zr_6O_{3.41}(OH)_{4.59}(BPDC\text{-}NHPro)_{4.25}(TFA)_{1.11}(Form)_{2.98}$
UiO-67-AcOH	$Zr_6O_{4.61}(OH)_{3.39}(BPDC)_{5.42}(AcOH)_{0.43}(Form)_{0.11}$
***o*-UiO-67-NH-Pro-AcOH**	$Zr_6O_{7.81}(OH)_{0.19}(BPDC\text{-}NHPro)_{3.0}(AcOH)_{0.02}(Form)_{2.16}$
***m*-UiO-67-NH-Pro-AcOH**	$Zr_6O_{5.0}(OH)_3(BPDC\text{-}NHPro)_{4.1}(AcOH)_{0.04}(Form)_{2.75}$
UiO-67-BA	$Zr_6O_{4.96}(OH)_{3.04}(BPDC\text{-}NHPro)_{4,78}(BA)_{1.43}(Form)_{0.05}$
***o*-UiO-67-NH-Pro-BA**	$Zr_6O_{5.89}(OH)_{2.11}(BPDC\text{-}NHPro)_{3.65}(BA)_{0.62}(Form)_{2.19}$
***m*-UiO-67-NH-Pro-BA**	$Zr_6O_{6.12}(OH)_{1.88}(BPDC\text{-}NHPro)_{3.48}(BA)_{0.49}(Form)_{2.43}$

4.5. Scanning Electron Microscopy (SEM)

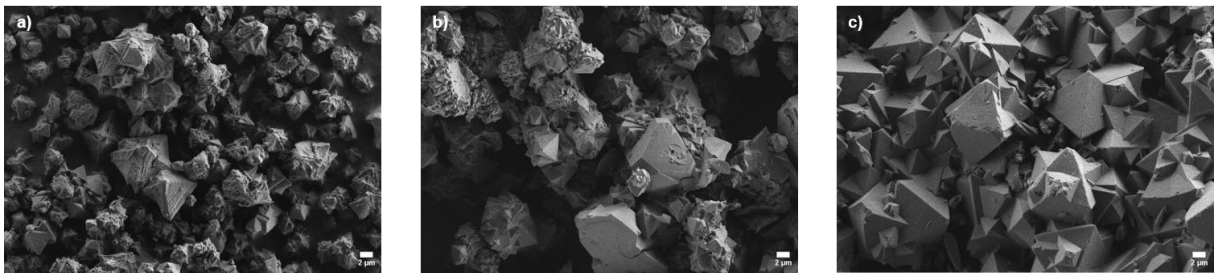

Figure S13: SEM micrographs of a) UiO-67-TFA, b) *o*-UiO-67-NH-Pro-TFA and c) *m*- UiO-67-NH-Pro-TFA.

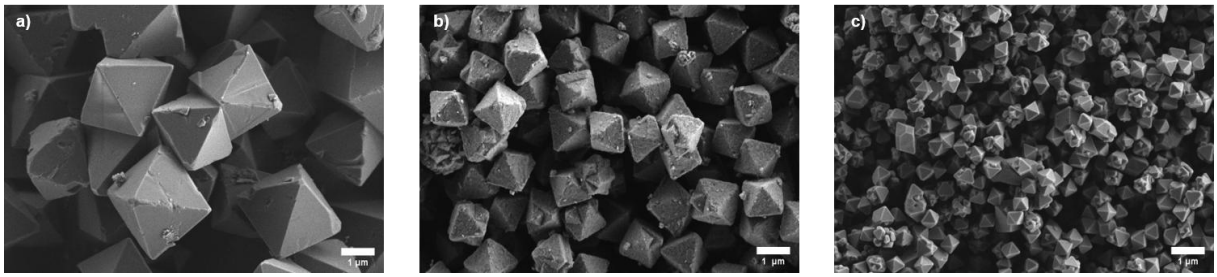

Figure S14: SEM micrographs of a) UiO-67-AcOH, b) *o*-UiO-67-NH-Pro-AcOH and c) *m*-UiO-67-NH-Pro-AcOH.

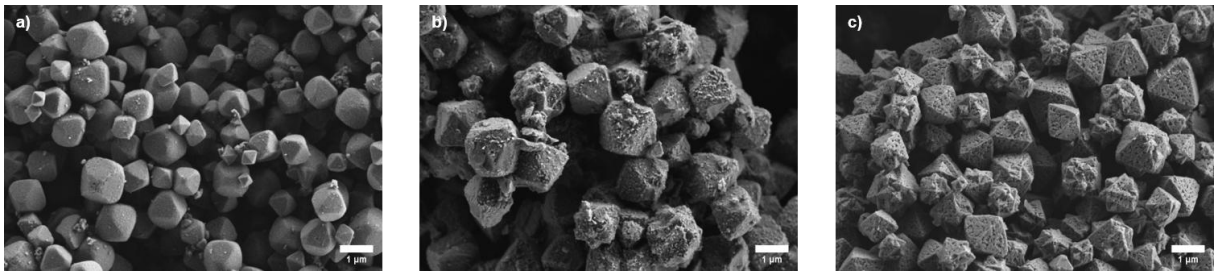

Figure S15: SEM micrographs of a) UiO-67-BA, b) *o*-UiO-67-NH-Pro-BA and c) *m*- UiO-67-NH-Pro-BA.

4.6. Stability of the catalysts

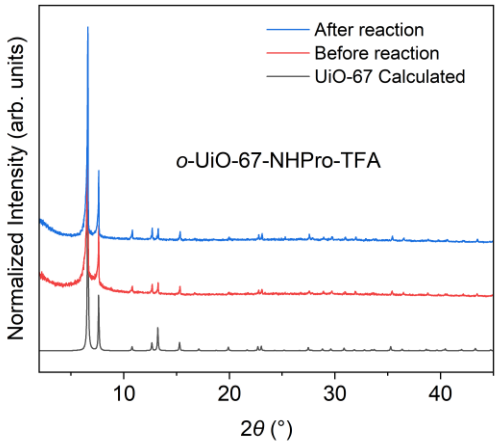

Figure S16: PXRD patterns of the *o*-UiO-67-NHPro-TFA before and after catalytic reaction.

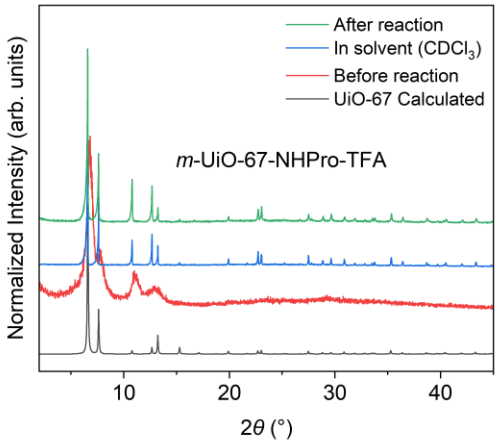

Figure S17: PXRD patterns of the *m*-UiO-67-NHPro-TFA before and after catalytic reaction. Since the MOF was losing long range order in the dry conditions, the pattern after re-immersing the catalyst in the reaction solvent is presented to confirm the crystallinity of the catalyst in reaction solution

5. Organocatalytic aldol additions

In order to compare the catalytic activity of homogenous catalysts ***o*-UiO-67-NH-Pro** with the known ***m*-UiO-67-NH-Pro**, the organocatalytic of aldol reaction of 4-nitrobenzaldehyde **7** with cyclohexanone **8** to the *syn*- and *anti*-aldol products *syn*-**9** and *anti*-**9** was studied as benchmark reaction (Scheme S3).

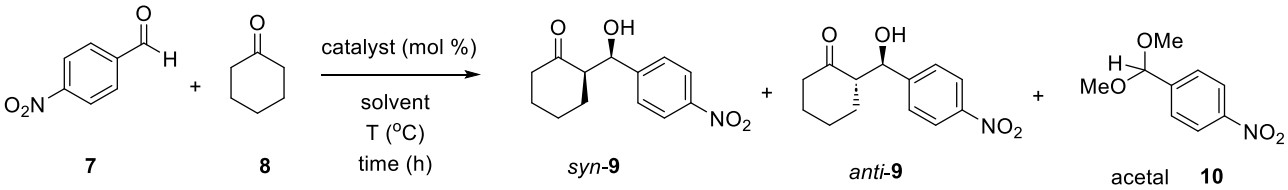

Scheme S3. General reaction conditions for asymmetric organocatalytic reaction of 4-nitro-benzaldehyde **7** with cyclohexanone **8** to aldol products *syn*-**9**, *anti*-**9** and acetal **10**.

The results of both homogeneous and heterogeneous catalysis are summarized in Table S4 and S6 correspondingly. First, the soluble proline-functionalized linkers *ortho*-**5**, *meta*-**5** were examined under homogeneous conditions. Taking previous work by Kaskel *et al.* [24] into account, we expected the heterogenous catalysis to proceed rather slowly and thus extended reaction times were applied for both homogeneous and heterogeneous reactions.

5.1. Organocatalytic aldol addition under homogeneous conditions

To a stirred solution of 4-nitrobenzaldehyde **7** (200 mg, 1.32 mmol), catalyst (20 mol%) in 2 mL solvent, cyclohexanone **8** (0.41 mL, 3.97 mmol) was added to start the reaction. The reaction mixture was left stirring at rt for 22 h. A saturated aqueous NH_4Cl solution (2 mL) was added and the aqueous layer was extracted with CH_2Cl_2 (2 × 20 mL). The combined organic layers were dried over $MgSO_4$, the solvent was removed under reduced pressure and the crude product was purified by column chromatography on silica (hexanes / EtOAc = 4 : 1) to give aldols **9** as a yellow solid. Diastereoselectivity was determined by ^1H NMR and *erf* values using HPLC with chiral stationary phase.

2-(Hydroxy(4-nitrophenyl)methyl)cyclohexan-1-one (9)

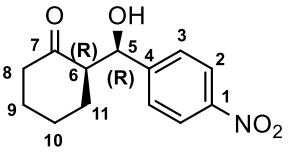

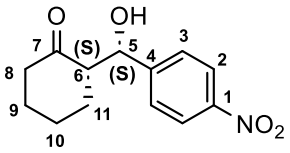

249.10 g/mol
$C_{13}H_{15}NO_4$

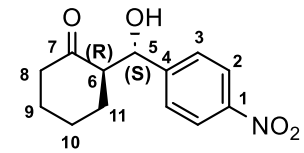

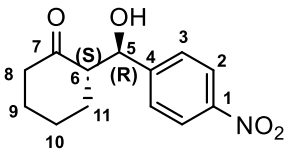

249.10 g/mol
$C_{13}H_{15}NO_4$

syn-**9** *anti*-**9**

syn-**9**: ^{1}H-NMR (400 MHz, $CDCl_3$): δ = 1.39-1.92 (m, 6H, H-9, H-10, H-11), 2.05−2.18 (m, 1H, OH), 2.37−2.67 (m, 3H, H-6, H-8), 5.49 (s, 1H, H-5, *syn*-H-5), 7.51 (d, *J* = 7.49 Hz, 2H, H-2), 8.21 (d, *J* = 8.83 Hz, 2H, H-1) ppm. ^{13}C-NMR (400 MHz, $CDCl_3$): δ = 24.7 (C-11), 27.6 (C-10), 30.8 (C-9), 42.7 (C-8), 57.20 (C-6), 74.0 (C-5), 123.6 (C-2), 127.6 (C-3), 147.6 (C-1), 148.4 (C-4), 214.7 (C-7) ppm.

anti-**9**: ^{1}H-NMR (400 MHz, $CDCl_3$): δ = 1.39-1.92 (m, 6H, H-9, H-10, H-11), 2.05−2.18 (m, 1H, OH), 2.37−2.67 (m, 3H, H-6, H-8), 4.89 (dd, *J* = 8.51, 3.03 Hz, 1H, H-5, *anti*-CH), 7.51 (d, *J* = 7.49 Hz, 2H, H-2), 8.21 (d, *J* = 8.83 Hz, 2H, H-1) ppm; ^{13}C-NMR (400 MHz, $CDCl_3$): δ = 24.7 (C-11), 27.6 (C-10), 30.8 (C-9), 42.7 (C-8), 57.20 (C-6), 74.0 (C-5), 123.6 (C-2), 127.6 (C-3), 147.6 (C-1), 148.4 (C-4), 214.7 (C-7) ppm.

The spectroscopic data are in accordance with literature.[25]

1-(Dimethoxymethyl)-4-nitrobenzene (**10**)

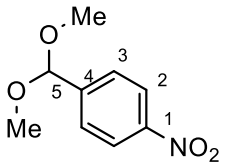

$C_9H_{11}NO_4$
197.19 g/mol

10

^{1}H NMR (300 MHz, $CDCl_3$) δ = 3.31 (s, 6H, OMe), 5.45 (s, 1H, H-5), 7.61 (d, *J* = 8.7 Hz, 2H, H-2), 8.19 (d, *J* = 8.7 Hz, 2H, H-3) ppm. ^{13}C NMR (75 MHz, $CDCl_3$) δ = 52.8 (OMe), 101.6 (C-5), 123.5 (C-3), 127.9 (C-2), 145.2 (C-1), 148.0 (C-4) ppm. The spectroscopic data are in accordance with literature.[26]

5.1.1. Kinetic study of organocatalytic aldol addition under homogeneous conditions

In an NMR tube, 4-nitrobenzaldehyde **7** (50 mg, 0.33 mmol), catalyst (20 mol%), cyclohexanone **8** (103 µL, 0.99 mmol) and mesitylene (46 µL, 0.33 mmol) were dissolved in 0.5 mL $CDCl_3$ at room temperature for 22 h. The conversion to aldol products **9** and *dr* was monitored via ^1H NMR as shown in Figure S18 and S19.

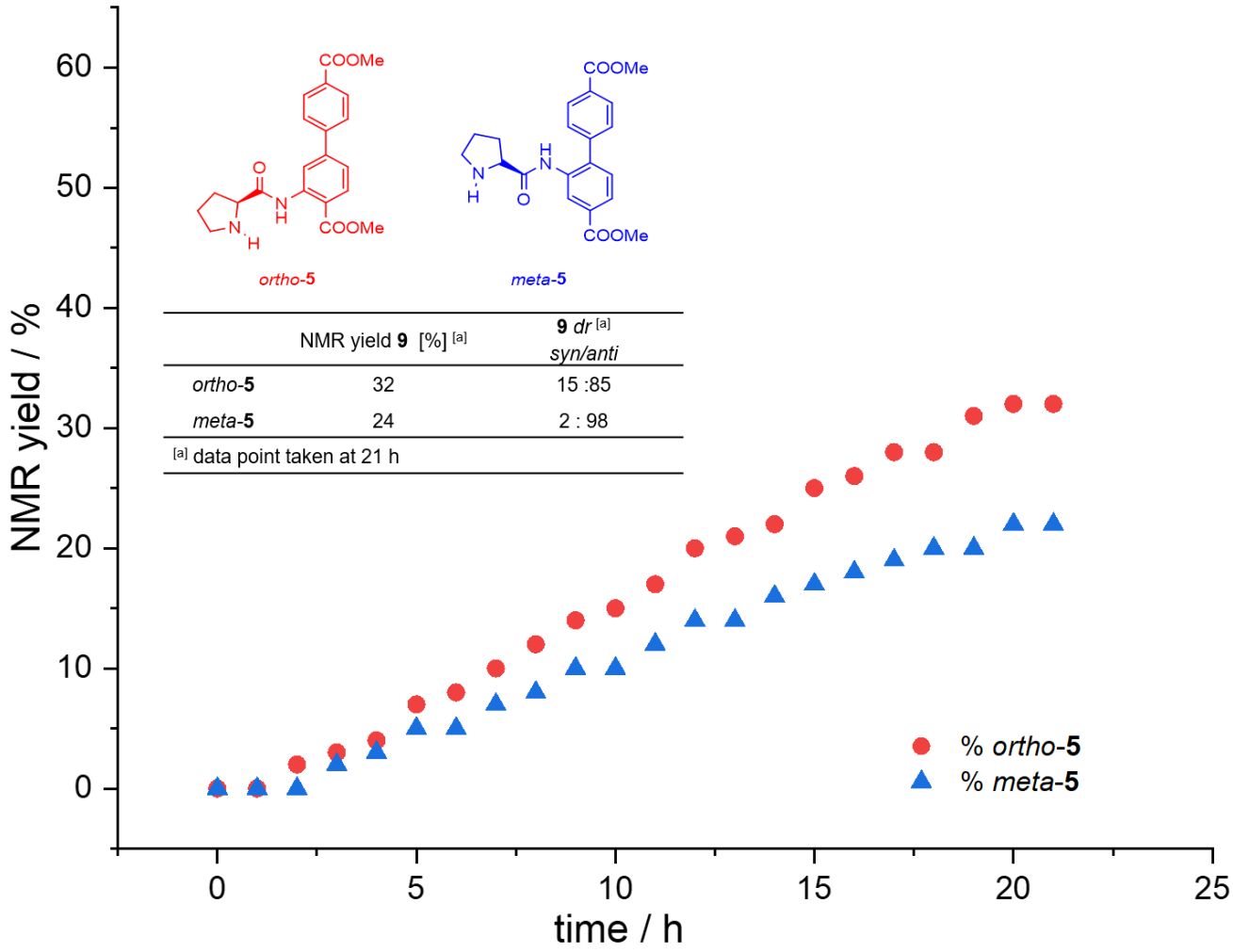

	NMR yield **9** [%] [a]	**9** *dr* [a] *syn/anti*
ortho-**5**	32	15 :85
meta-**5**	24	2 : 98

[a] data point taken at 21 h

Figure S18: Organocatalytic aldol addition in the presence of 5 mol% loading of soluble catalysts *ortho*-**5** *and meta*-**5**.

5.1.2. Comparison of ^{1}H NMR spectra of aldol products (9) and acetal (10)

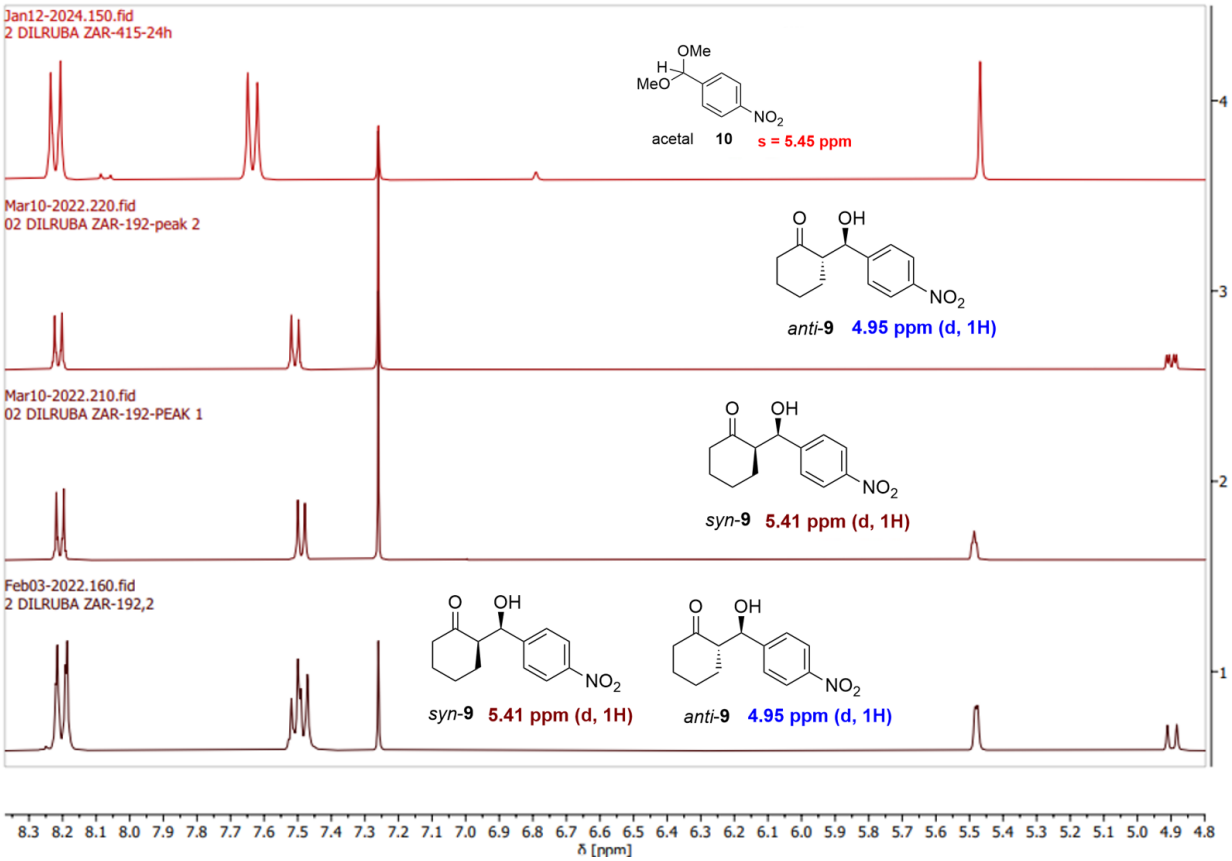

Figure S19: Sections of the ^{1}H NMR spectra (300 MHz, $CDCl_3$) of a) acetal **10**, b) *anti*-**9** c) *syn*-**9**, d) mixture of *anti*-**9**, *syn*-**9**.

5.1.3. Effect of acid additives on the aldol addition under homogeneous conditions

The effect of various acid additives i.e. Trifluoracetic acid (TFA), benzoic acid (BA) and acetic acid (AcOH) was also investigated under homogenous conditions and the results are summarized in Table S3.

Table S3. Effect of acid additives on the organocatalytic aldol addition under homogenous conditions.

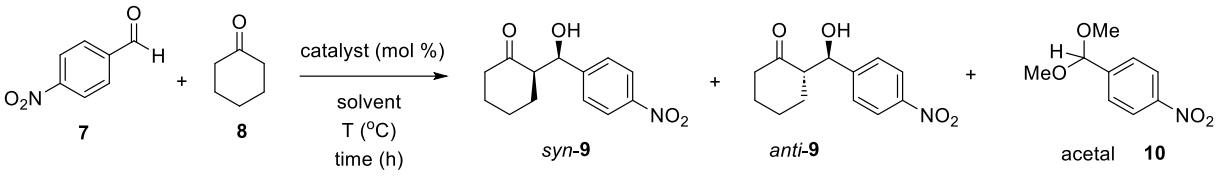

Entry	solvent (5 mL)	acid additive (0.2 equiv.)	T (°C)	aldol **9** [%] [a]	acetal **10** [%] [a]
(1)	MeOH	-	40	0	0
(2)	MeOH	TFA	r.t.	0	95
(3)	MeOH	TFA	40	0	96
(4)	MeOH	BA	r.t.	traces	0
(5)	MeOH	BA	40	traces	-
(6)	$CDCl_3$	TFA	40	traces	0
(7)	$CDCl_3$	BA	40	traces	0
(8)	$CDCl_3$	AcOH	40	traces	0
(9)	EtOH	AcOH	40	traces	0

[a] ^{1}H NMR yield was determined by integration of the characteristic benzylic protons in the crude mixture (aldol 7.48 ppm (d, 2H), acetal **10**: 7.63 ppm (d, 2H).

Table S4. Preliminary experiments on homogenous organocatalytic aldol addition of 4-nitrobenzaldehyde ***7*** and cyclohexanone **8** under various conditions.

Entry	Catalyst	time [d]	solvent	mol%	yield [a] **9** [%]	yield [a] **10** [%]	**9** *dr* [a] *syn*/*anti*	*syn*-**9** *er* [b, c] *min./maj.*	*anti*-**9** *er* [b] *(R,S/ S,R)*
(1)	*ortho*-**5**	7	$CDCl_3$	5	15	0	27 : 73	43 : 57	41 : 59
(2)	*ortho*-**5**	7	MeOH	5	22	40	40 : 60	59 : 41	27 : 73
(3)	*ortho*-**5**	7	DMSO	5	26	0	33 : 67	56 : 44	27 : 71
(4)	*ortho*-**5**	1	$CDCl_3$	20	>99	0	20 : 80	44 : 56	36 : 64
(5)	*meta*-**5**	9	$CDCl_3$	5	7	0	38 : 62	35 : 65	9 : 91
(6)	*meta*-**5**	7	MeOH	5	6	15	13 : 87	43 : 57	17 : 83
(7)	*meta*-**5**	7	DMSO	5	5	0	29 : 71	41 : 59	22 : 78
(8)	*meta*-**5**	3	$CDCl_3$	20	>99	0	25 : 75	59 : 41	20 : 80

[a] determined from the ^{1}H NMR spectrum of the crude product using mesitylene as the external standard. [b] determined by HPLC on a CHIRALPAK® AD-H column, 250 x 4.6 mm, 5 µm, hexane : *i*-PrOH (90:10), 0.8 mL/min, 254 nm, 22 °C. [c] *syn*-**9**: minor (*R,R*) or (*S,S*), major (*S,S*) or (*R,R*); all reactions were performed at 40 °C.

In order to rationalize the reversal of the diastereoselectivity (and the varying enantioselectivity) the published catalytic cycle of the proline-catalyzed aldol reaction has to be considered (Scheme S5),[28-30] where initial condensation to the iminium ion **S11** is followed by iminium ion-to-enamine equilibrium, subsequent aldol reaction with concomitant formation of the stereogenic centers and final enamine hydrolysis to the aldol products *syn*-**9**, *anti*-**9**.

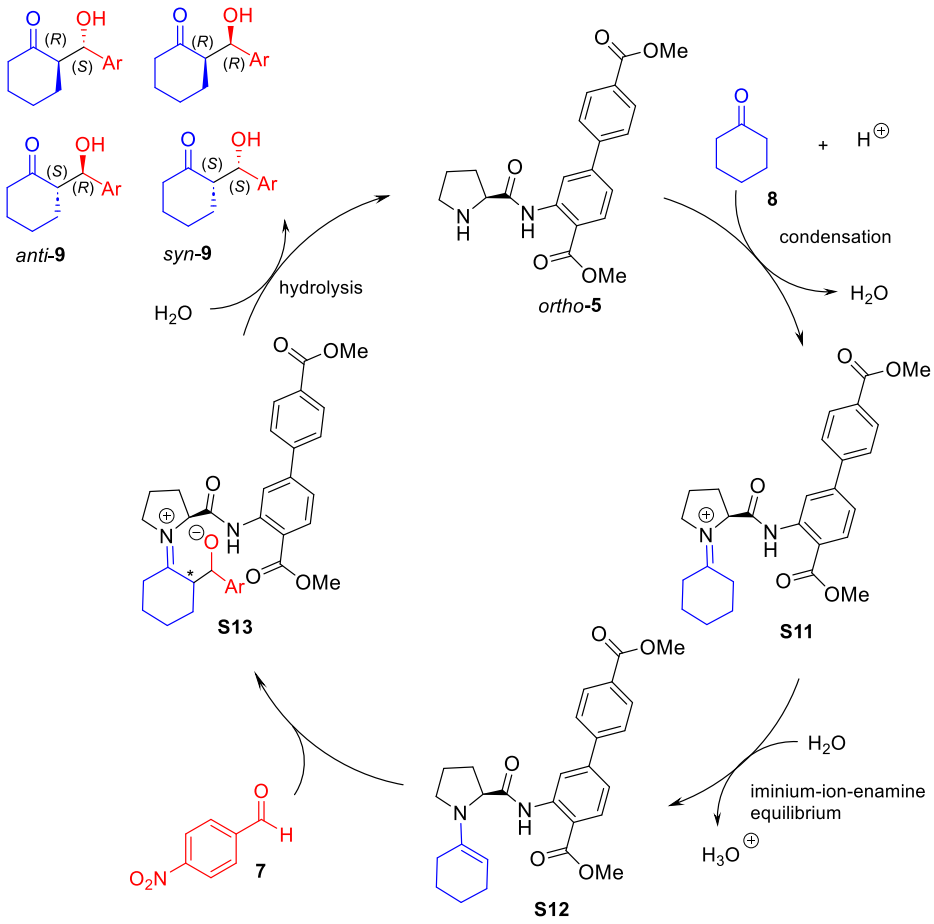

Scheme S4: Catalytic cycle of the proline-catalyzed aldol reaction[28-30]

For the homogeneous aldol reaction in the presence of soluble *ortho*-**5** four cyclic transition states **TS1** – **TS4** are conceivable (Scheme 5), where the aldehyde **7** is H-bonded to the amide N-H of the organocatalyst. In **TS1** *Si*-attack of enamine at the *Si*-face of the aldehyde suffers from steric hindrance between the aldehyde aryl unit Ar and the methyl ester of the biphenyl unit. **TS1** leads to *anti*-(*R,S*)-**9**.

In **TS2** *Re*-attack of enamine at the *Re*-face of the aldehyde leads to the enantiomeric *anti*-aldol *anti*-(*S,R*)-**9**. Contrary to **TS1**, **TS2** can be stabilized by π–π interactions between the aldehyde aryl unit Ar and the biphenyl, which might explain the observed preference of enantiomer *anti*-(*S,R*)-**9** over *anti*-(*R,S*)-**9** (Table 1, entries 1 – 7). On the other hand, in **TS3***Si*-attack of enamine at the *Re*-face of the aldehyde leading to *syn*-(*R,R*)-**9** should be disfavoured due to steric interactions between the aldehyde aryl Ar and the cyclohexenyl ring of the

enamine. A similar steric hindrance is also observed in **TS4**, where *Re*-attack of enamine at the *Si*-face of the aldehyde leads to *syn*-(*S,S*)-**9**. Thus, both *syn*-aldols are disfavoured against the *anti*-aldols. Furthermore, the interactions in **TS3**, **TS4** differ only little and thus no enantioselectivity was observed for the *syn*-aldols.

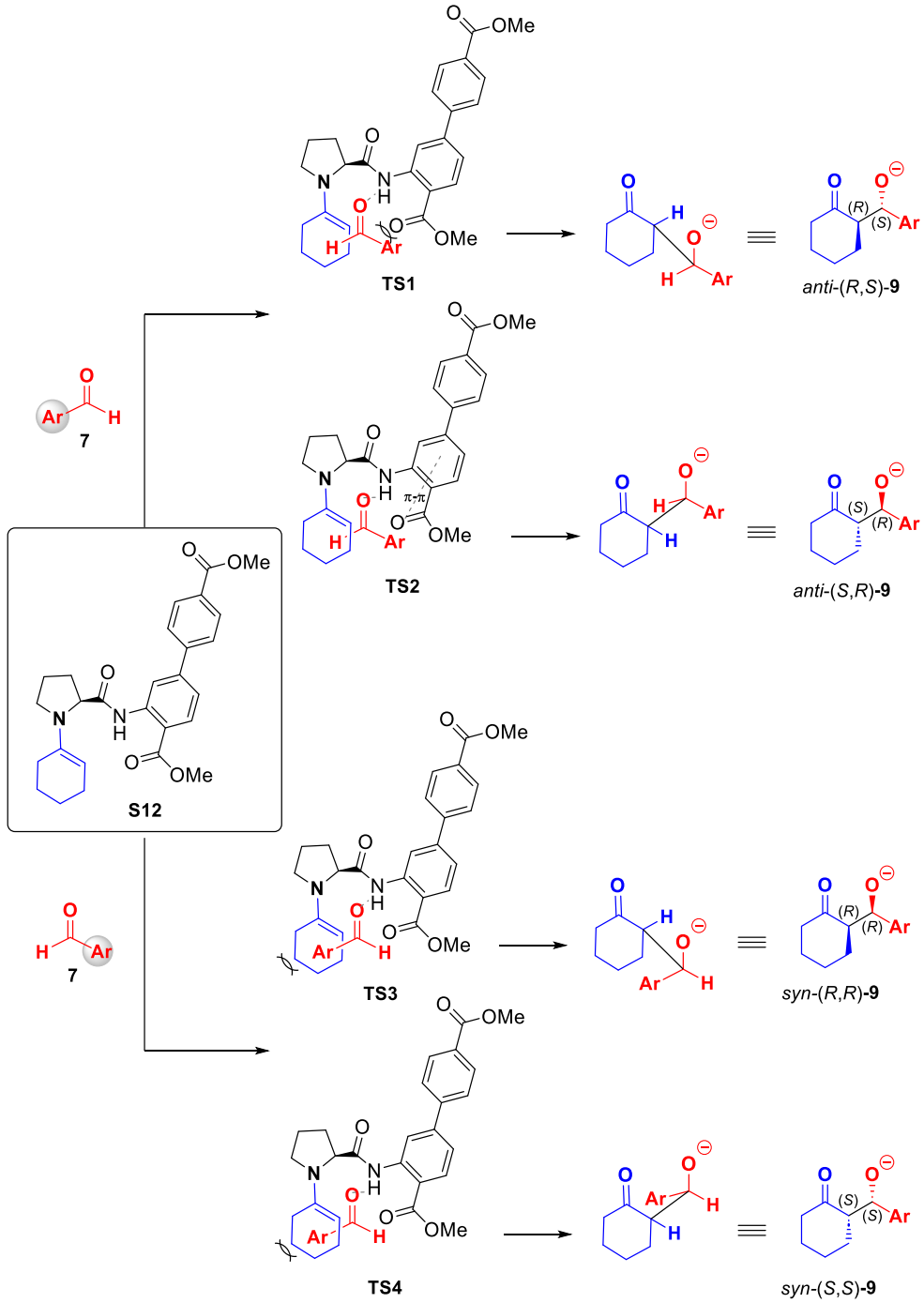

Scheme S5: Proposed transition states of the homogeneous catalysis to rationalize the stereochemistry.

5.2. Organocatalytic aldol addition under heterogeneous conditions

Aldol reaction of 4-nitrobenzaldehyde **7** (151 mg, 1.0 mmol) and cyclohexanone **8** (1.04 mL, 10 mmol) in 5 mL MeOH with 20 mg of Zr-MOF catalyst ***o*-UiO-67-NH-Pro-TFA** (5 mol%) was carried out under direct stirring at 40 °C. The reaction mixture was stirred for several d at 40 °C and the conversion was monitored at different time intervals via ^{1}H NMR. For each measurement, 0.1 mL of sample was removed from the reaction mixture using PTFE syringe filter (Ø = 13 mm, pore sizes = 0.22 µm). ^{1}H NMR yield was determined by integration of the characteristic benzylic protons in the crude mixture (aldehyde **7** : 10.1 ppm (s, 1H), aldol **9** : 7.48 ppm (d, 2H), acetal **10** : 7.63 ppm (d, 2H). Diastereoselectivity (*dr*) was determined by achiral HPLC and enantioselectivity, i.e. *er* values using chiral HPLC. Results are shown in Table S6.

Table S5. Preliminary optimization experiments on heterogeneous organocatalytic aldol addition with the Zr-MOF catalyst ***o*-UiO-67-NH-Pro-TFA**.

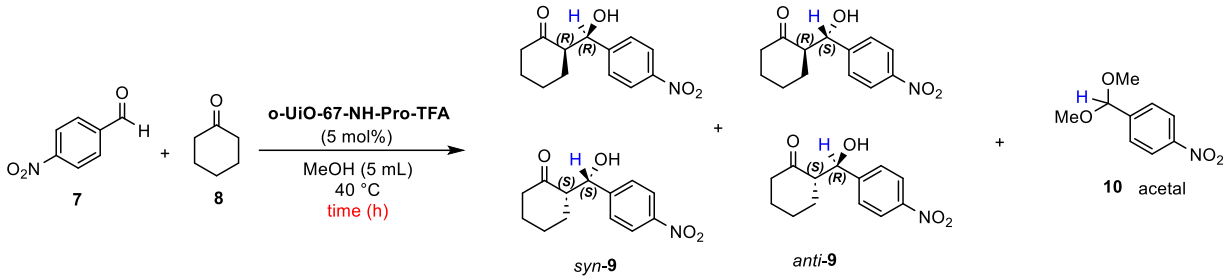

entry	time [d]	aldol **9** [%] [a]	acetal **10** [%] [a]	**9** *dr* [b] *syn/anti*	*er syn*-**9** [c] *min./maj.*	*er anti*-**9** [c] (*R,S/S,R*)
(1)	0.5 h	0	0	-	-	-
(2)	1	3	2	-	-	-
(3)	2	4	5	-	-	-
(4)	3	5	6	-	-	-
(5)	4	6	7	97 : 3	n.d. [e]	33 : 67
(6)	7	9	9	90 : 10	42 : 58	35 : 65
(7)	9	11	14	84 : 16	n.d. [e]	n.d. [e]
(8)	11	12	18	86 : 14	52 : 48 [d]	45 : 55 [d]

[a] ^{1}H NMR yield was determined by integration of the characteristic benzylic protons in the crude mixture (aldehyde **7**: 10.1 ppm (s, 1H), aldol **9**: 7.48 ppm (d, 2H), acetal **10**: 7.63 ppm (d, 2H)). [b] *dr* was determined by achiral HPLC (kromasil 90 : 10, 1ml / min). [b] *er* was determined using chiral HPLC (CHIRALPAK AD-H, hexane : 2-propanol (90 : 10) ; 0.8 ml / min) and *syn*-**9**: minor (*R,R*) or (*S,S*), major (*S,S*) or (*R,R*) in agreement with ref. [27]; [d] isolated produc [e] poor separation via HPLC

Table S6. Heterogeneous organocatalytic aldol addition with different catalysts and varying conditions.

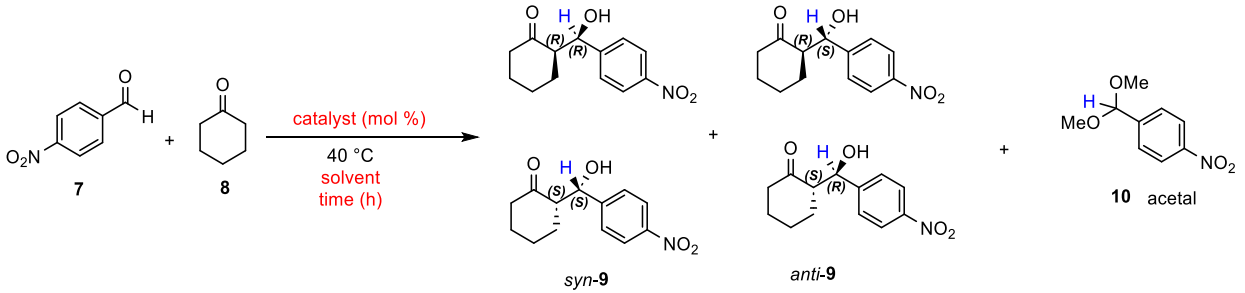

Entry	Catalyst	time [d]	Solvent	mol%	yield [a] **9** [%]	yield [a] **10** [%]	**9** *dr* [a] *syn*/*anti*	*syn*-**9** *er* [b, c] *min./maj.*	*anti*-**9** *er* [b] *(R,S/ S,R)*
(1)	**UiO-67-AcOH** (0% Pro)	7	$CDCl_3$	5	12	0	75 : 25	50 : 50	53 : 47
(2)	**UiO-67-TFA** (0% Pro)	7	$CDCl_3$	5	9	0	81 : 19	50: 50	52 : 48
(3)	**UiO-67-TFA** (0% Pro)	7	$CDCl_3$	20	60	0	79 : 21	50 : 50	52: 48
(4)	***o*-UiO-67-NH-Pro-AcOH**	7	$CDCl_3$	5	4	0	67 : 33	48 : 52	54 : 46
(5)	***o*-UiO-67-NH-Pro-BA**	7	$CDCl_3$	5	3	0	71 : 29	50 : 50	-
(6)	***o*-UiO-67-NH-Pro-TFA**	7	$CDCl_3$	5	4	0	73 : 27	49 : 51	-
(7)	***o*-UiO-67-NH-Pro-TFA**	7	MeOH	5	9	9	91 : 9	42 : 58	65 : 35
(8)	***o*-UiO-67-NH-Pro-TFA**	16	MeOH	5	4	34	95 : 5	50 : 50	50 : 50
(9)	***m*-UiO-67-NH-Pro-AcOH**	7	$CDCl_3$	5	<1	-	-	-	-
(10)	***m*-UiO-67-NH-Pro-BA**	7	$CDCl_3$	5	12	0	71 : 29	50 : 50	60 : 40
(11)	***m*-UiO-67-NH-Pro-TFA**	7	$CDCl_3$	5	4	0	69 : 31	49 : 51	56 : 44
(12)	***m*-UiO-67-NH-Pro-TFA**	7	MeOH	5	5	75	61 : 39	56 : 44	95 : 05
(13)	$ZrOCl_2 \cdot 8H_2O$	7	$CDCl_3$	15	5	0	54 : 46	47 : 53	46 : 54
(14)	$ZrOCl_2 \cdot 8H_2O$	20 h	MeOH	15	0	96	-	-	-

[a] ^{1}H NMR yield was determined by integration of the characteristic benzylic protons in the crude mixture (aldehyde **7**: 10.1 ppm (s, 1H), aldol **9**: 7.48 ppm (d, 2H), acetal **10**: 7.63 ppm (d, 2H). [b] *dr* was determined by achiral HPLC (kromasil 90 : 10, 1ml / min) and *er* was determined using chiral HPLC (CHIRALPAK AD-H, hexane : 2-propanol (90 : 10) ; 0.8 ml / min) and *syn*-**9**: minor (*R,R*) or (*S,S*), major (*S,S*) or (*R,R*) in agreement with ref. [27]; [d] isolated product; [e] poor separation via HPLC.

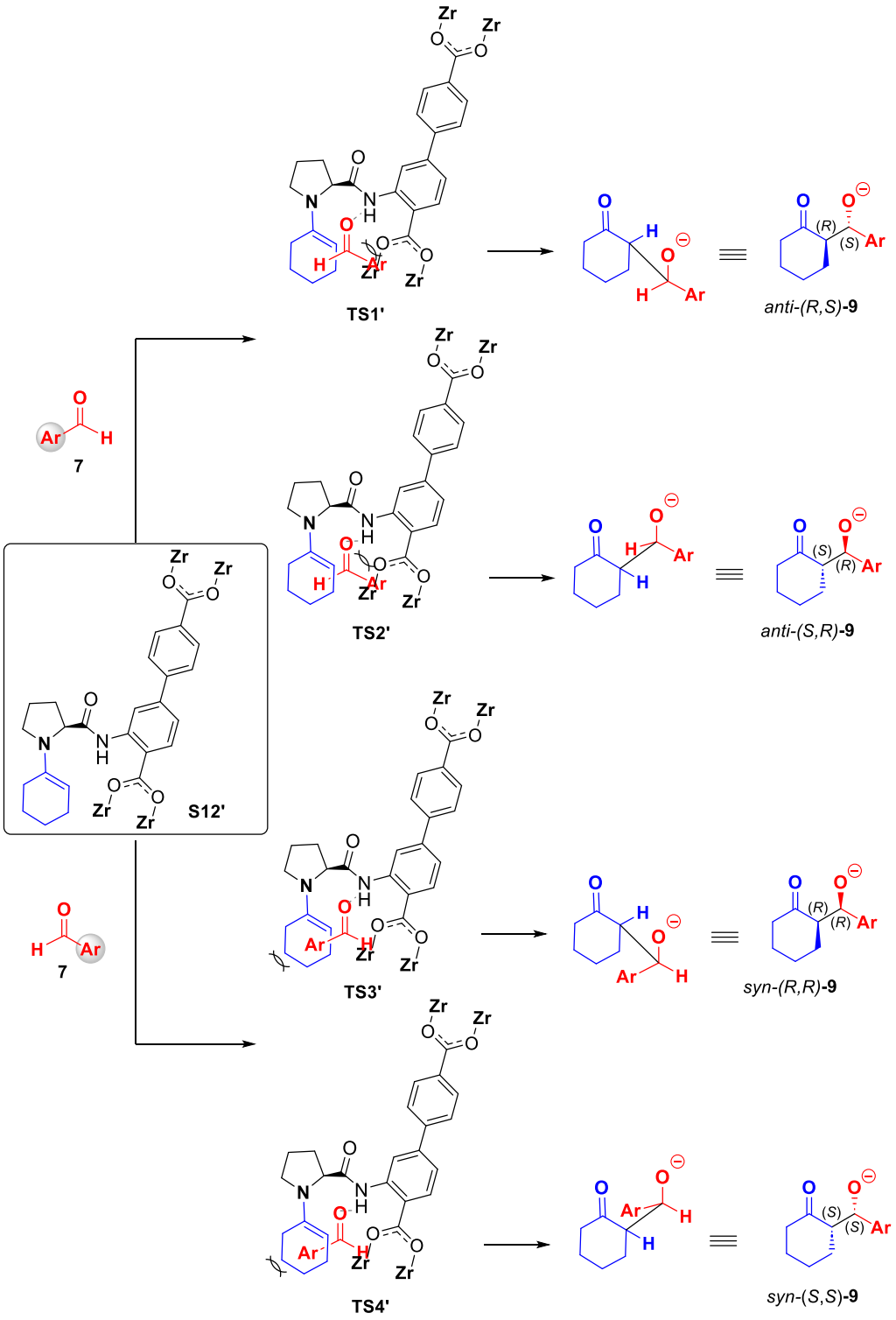

Scheme S6: Proposed transition states of the heterogeneous catalysis to rationalize the stereochemistry.

In contrast to the homogeneous case **TS1‘** and **TS2‘** suffer from severe steric hindrance between the aldehyde aryl Ar and the Zr node. For the heterogeneous aldol reaction four cyclic transition states **TS1‘** – **TS4‘** might be proposed (Scheme S6), where the aldehyde is connected to the amide N-H of the enamine via H-bond. In other words, the confinement strongly disfavors the *anti*-diastereomers *anti*-(*R,S*)-**9**, *anti*-(*S,R*)-**9**, regardless of *Si,Si*-attack or *Re,Re*-attack (resulting in racemic *anti*-aldols). On the other hand, in **TS3‘** and **TS4‘** steric hindrance between the cyclohexenyl ring of the enamine and the aryl unit is present, while steric hindrance between the aldehyde and the Zr node is absent. This might explain the preferred formation of the *syn*-aldols, albeit at a reduced reaction rate as compared to the homogeneous reaction. Moreover, there is little difference between the interactions in **TS3‘** and **TS4‘** (or **TS1‘** and **TS2‘**) and thus almost racemic *syn*- and *anti*-aldols were formed under heterogeneous catalysis respectively (Table 1, entries 8 – 13). Alternatively, transition states **TS3“** and **TS4“** might be proposed, where the Zr node acts as a Lewis acid coordinating the aldehyde carbonyl group (Scheme S7).

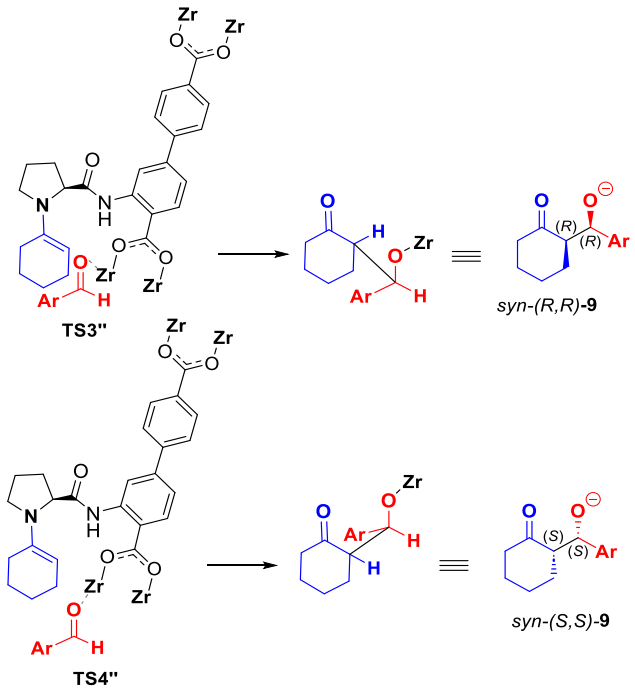

Scheme S7: Alternative transition states of the heterogeneous catalysis.

For example, in **TS3“** *Si*-attack of the enamine to the *Re*-face of the aldehyde should lead to the *syn*-(*R,R*)-**9**, while the enantiomeric *syn*-aldol *syn*-(*S,S*)-**9** is generated via *Si*,*Re*-attack in **TS4“**.

5.2.1. Hot filtration test

For hot filtration tests, the aldol reaction of **7** (151 mg, 1.0 mmol) and **8** (1.04 mL, 10 mmol) in 5 mL solvent were performed under direct stirring with Zr-MOF catalysts at 40 °C. After 48 h, the solid catalyst was removed from reaction mixture using PTFE syringe filter (Ø = 13 mm, pore sizes = 0.22 µm). The mixture was stirred several d at 40 °C, and the progress of the reaction was tracked by periodically extracting 0.1 mL samples for analysis using ^{1}H NMR. Yields were determined by integration of the characteristic benzylic protons in the crude mixture (aldehyde **7** : 10.1 ppm (s, 1H), aldol **9** : 7.48 ppm (d, 2H), acetal 10 : 7.63 ppm (d, 2H). Diastereoselectivity (*dr*) was determined by achiral HPLC and enantioselectivity values using chiral HPLC.

Hot filtration tests showed, that upon removal of the solid catalyst after 48 h, the concentration of aldols **9** remained constant but the formation of acetal **10** kept increasing (Figure S20a), confirming the heterogeneous character of the catalyst, whereas the acetal concentration increased steadily even in the absence of MOFs (Figure S20 b). In Figure 3 in the manuscript, the comparison hot filtration of **UiO-67-TFA**, ***o*-UiO-67-NH-Pro-TFA** and ***m*-UiO-67-NH-Pro-TFA** is depicted.

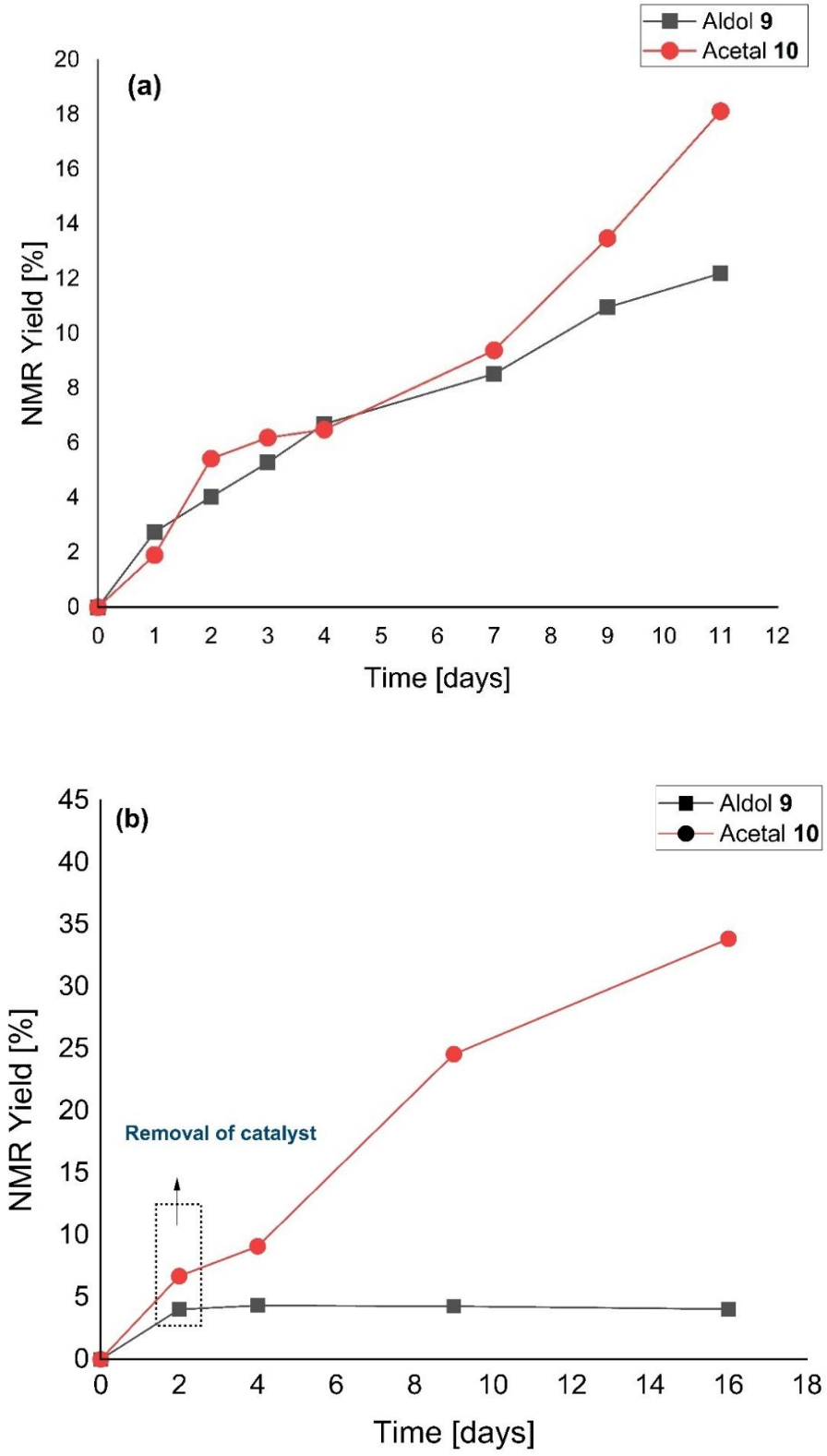

Figure S20: NMR yields of the products. a) Yields of aldols **9** and acetal **10** in the presence of 5 mol% of ***o*-UiO-67-NH-Pro-TFA** in MeOH. b) Yields of aldol **9** and acetal **10** in the presence of 5 mol% of ***o*-UiO-67-NH-Pro-TFA** in MeOH after removal of the MOF via hot filtration after 48 hours.

6. MD simulations and DFT-optimization of the metal cluster

6.1. Computational methods

The geometry of the metal cluster (visualized in Figure S21) was optimized by density functional theory (DFT) using the B3LYP-D3(BJ) functional and the def2-SVP basis set.[1-5] The DFT calculation was performed using Turbomole V7.4.1 [6] in ChemShell [7] [8] via DL-FIND.[9] The initial geometry was taken from.[10]

To study the movement and interactions of the solvent molecules, reactants, and products within the **UiO-67** MOFs, all-atom molecular dynamics (MD) simulations were performed using GROMACS 2016 [11] and the CHARMM force field [12,13]. For this purpose, one-unit cell of **UiO-67** was inserted into a simulation box, thus containing four metal clusters and 4,4'-biphenyldicarboxylic acid (H4BPDC) linkers with or without the proline-catalyst in the *meta* and *ortho* position. [14a] In order to study the impact of structural defects on the system, additional simulation systems were constructed, where missing linker defects were introduced (see Figures S22-26). Specifically, in each system – the MOF without the proline catalyst, as well as the systems with proline in the meta and ortho position – one or two linkers were removed and replaced with two trifluoroacetic acid (TFA) molecules per missing linker. Notably, in the systems with two removed linkers, a single linker in each of the two octahedral pores in the simulation unit cell were removed, ensuring a balanced defect distribution. Making usage of the fact that **UiO-67** is a rigid MOF, the positions of the metal cluster atoms as well as the oxygen atoms of the carboxyl group of the linkers were kept in constant position by the freeze algorithm. The remaining linker atoms could move freely. The freezing of the metal center enabled us to remove the bonds between the metal cluster and the linkers and thus to generate the force field parameters individually for the linkers, metal centers, methanol, reactants and products using CHARMM-GUI.[11,13] The Zr^{4+} atoms and the O^{2-} in between them were represented as dummy atoms interacting with the surroundings only via electrostatics. Next, the optimal number of methanol molecules per unit cell was calculated using Zeo^{++} [14b] for each simulation system. Unit cell parameters were taken from [15]. Simulation systems were prepared such that each system contained either both reactants **7** and **8** or the major product *syn*-**9**, as well as methanol molecules. Summary of all performed MD simulations can be found in Table S7.

The MD systems were energy minimized for 5000 steps using the steepest descent algorithm. Then velocities were generated at 310 K and an equilibration simulation of 0.25 ns was performed with a time step of 1 fs under the NVT ensemble, using a temperature of 313 K and the Berendsen thermostat.[16] Total production run simulation time of 30 µs for each system was collected under same conditions. Additional simulations (total production simulation time of 15 µs per ***o*-UiO-67-NH-Pro** and ***m*-UiO-67-NH-Pro** in both catalyst-containing MOFs with the

product were performed at a temperature of 813 K. In all simulations, electrostatics beyond the 1.2 nm cut-off were treated using the particle-mesh Ewald method. [17] Van der Waals forces were switched to zero between 0.8 and 1.2 nm with the potential-switch algorithm. The Verlet cut-off scheme with 0.005 kJ mol^{-1} ps^{-1} buffer tolerance was applied[18], and bonds to hydrogens were constrained using the LINCS algorithm[19]. The associated data will be provided by the DaRUS repository afterwards. Molecules were visualized in PyMOL. Plots were generated using Matplotlib[20].

6.2. Analysis of MD simulations and DFT-optimized geometry of the metal cluster

The distribution of distances from the active NH-group of the catalyst to the Zr atom in the metal cluster was studied in the ***o*-UiO-67-NH-Pro** and ***m*-UiO-67-NH-Pro** frameworks. Zeo^{++} [14] was used to calculate the accessible volume for all structures. The mean accessible volume and its standard deviation was estimated from 100 frames extracted each 100 ns from a 10 µs-long simulation. The average traveled distance of methanol, both reactants, and the product in all MOF structures was calculated for each simulation by analyzing the distance each molecule traveled in 1 µs. Additionally, the number of transitions of the product from pore to pore per 1 µs at 313 K was estimated from visual observations of the individual trajectories.

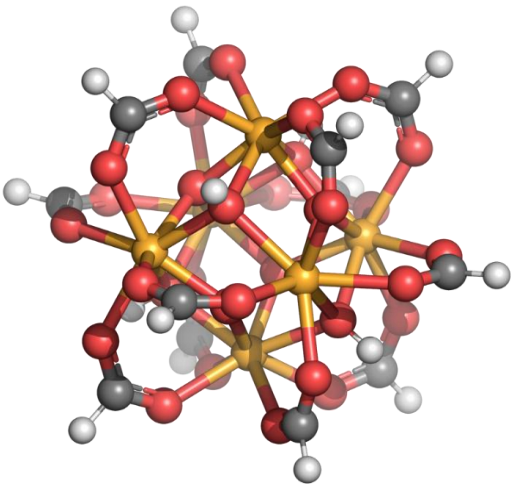

Figure S21: DFT-optimized geometry of the metal cluster $[Zr_6O_4(OH)_4]C_{12}O_{24}H_{12}$. Oxygen atoms are shown in red, zirconium in yellow, carbon in blue and hydrogen in white.

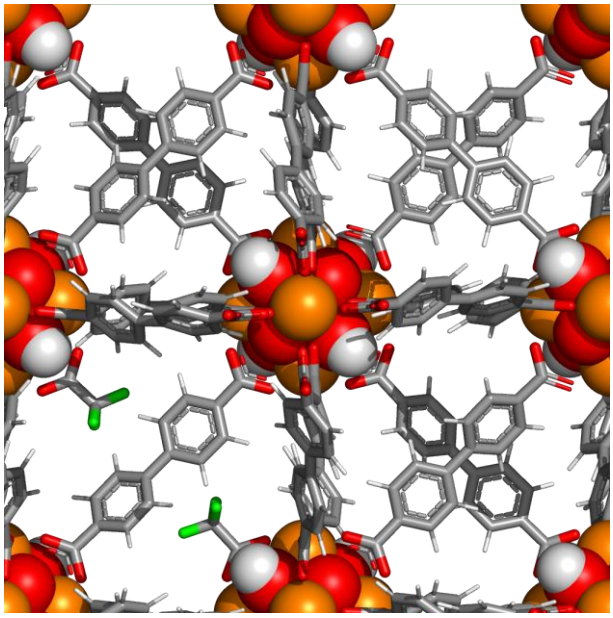

Figure S22: UiO-67 with one linker per unit cell substituted by two TFAs. The carbon atoms are grey, oxygens red, zirconium orange, hydrogens white and fluorine green.

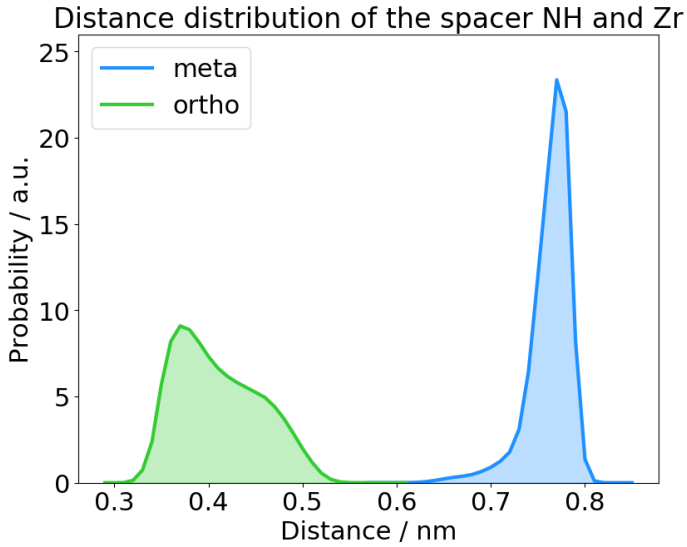

Figure S23: Minimal distance distributions of the NH-group of the enamine "spacer" to the Zr atom of the metal cluster in respect of catalyst

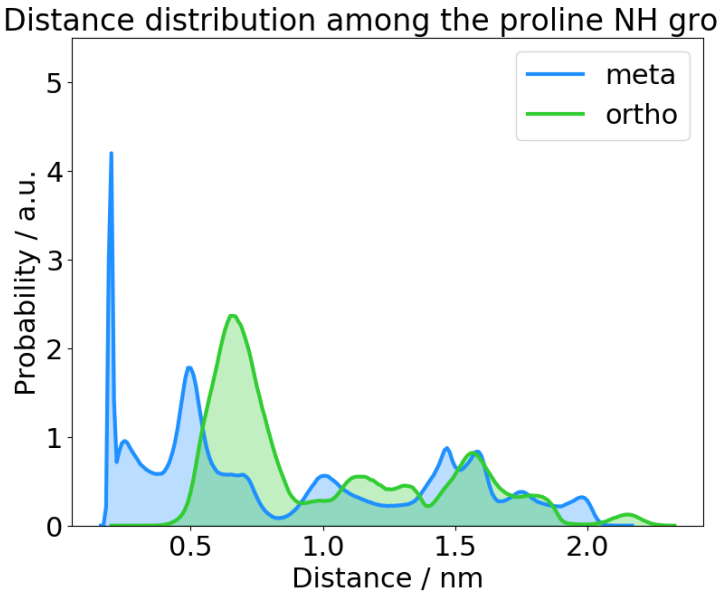

Figure S24: Minimal distance distributions of the NH-group of the enamine "spacer" to the Zr atom of the metal cluster in respect of catalyst position in defect-free MOFs.

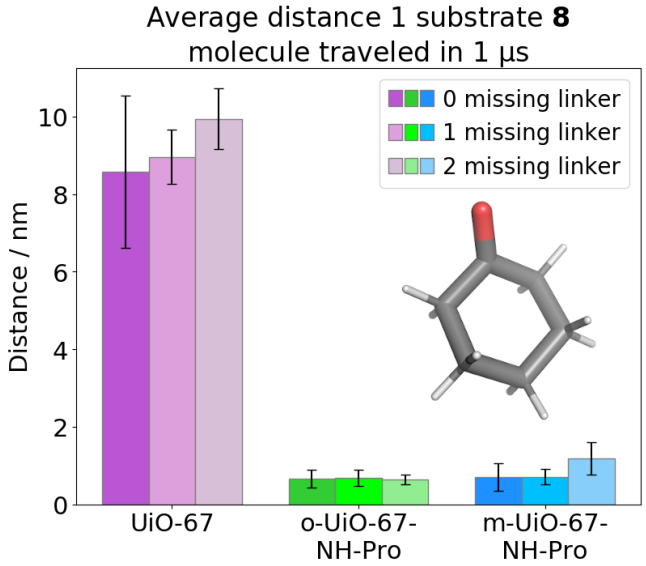

Figure S25: Average distance the substrate **8** covered in 1 µs in each system. The errors denote standard deviations.

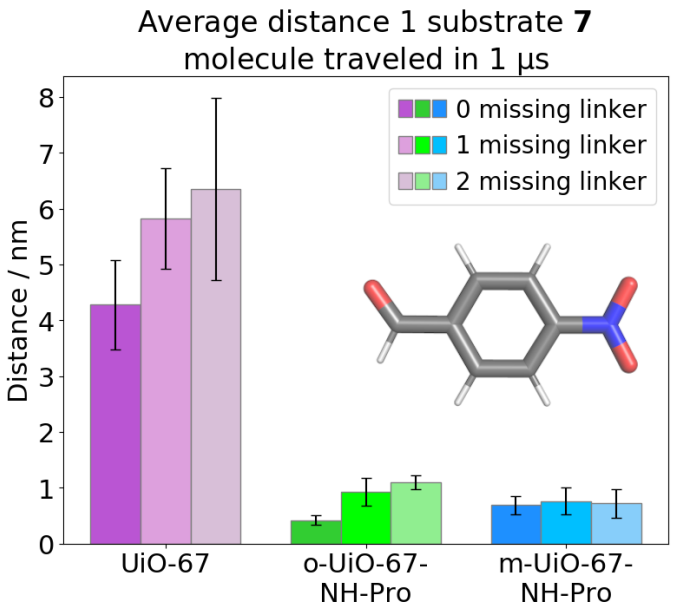

Figure S26: Average distance the substrate **7** covered in 1 µs in each system. The errors denote standard deviations.

Table S7. List of all performed all-atom MD simulations. Solutes are either reactants **7** + **8** or the *syn*-**9** product.

MOF	Solute	# MeOH	Temp.	# Simulations & Sim. time
UiO-67	**7** + **8**	172	313 K	6 x 5 µs
	syn-**9**	172	313 K	3 x 10 µs
UiO-67 1 missing linker / 2 TFA	**7** + **8**	183	313 K	6 x 5 µs
	syn-**9**	183	313 K	6 x 5 µs
UiO-67 2 missing linker / 4 TFA	**7** + **8**	184	313 K	6 x 5 µs
	syn-**9**	184	313 K	6 x 5 µs
***o*-UiO-67-NH-Pro**	**7** + **8**	121	313 K	6 x 5 µs
	syn-**9**	121	313 K	3 x 10 µs
	syn-**9**	121	813 K	3 x 5 µs
***o*-UiO-67-NH-Pro 1 missing linker / 2 TFA**	**7** + **8**	137	313 K	6 x 5 µs
	syn-**9**	137	313 K	6 x 5 µs
***o*-UiO-67-NH-Pro 2 missing linker / 4 TFA**	**7** + **8**	138	313 K	6 x 5 µs
	syn-**9**	138	313 K	6 x 5 µs
***m*-UiO-67-NH-Pro**	**7** + **8**	121	313 K	6 x 5 µs
	syn-**9**	121	313 K	3 x 10 µs
	syn-**9**	121	813 K	3 x 5 µs
***m*-UiO-67-NH-Pro 1 missing linker / 2 TFA**	**7** + **8**	137	313 K	6 x 5 µs
	syn-**9**	137	313 K	6 x 5 µs
***m*-UiO-67-NH-Pro 2 missing linker / 4 TFA**	**7** + **8**	138	313 K	6 x 5 µs
	syn-**9**	138	313 K	6 x 5 µs

7.

HPLC chromatograms

SHIMADZU LabSolutions **Analysis Report**

<Sample Information>

Sample Name	: 4-nitro-benzaldehyde_kromasil_90_10_1.0		
Sample ID	: 4-nitro-benzaldehyde_kromasil_9		
Data Filename	: 4-nitro-benzaldehyde_kromasil_90_10_1.0.lcd		
Method Filename	: GRA-140_ODH_98_2_1.0.lcm		
Batch Filename	:		
Vial #	: 1-77	Sample Type	: Unknown
Injection Volume	: 15 uL		
Date Acquired	: 16.01.2024 10:48:14	Acquired by	: System Administrator
Date Processed	: 16.01.2024 11:14:57	Processed by	: System Administrator

<Chromatogram>

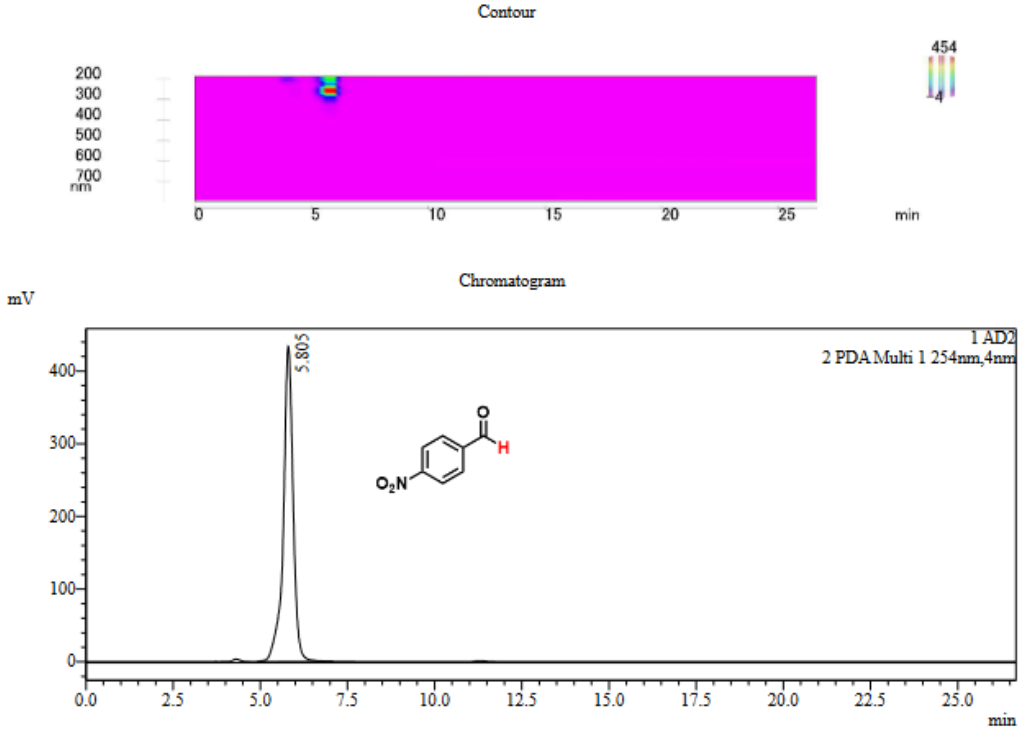

Peak Table

AD2

Peak#	Ret. Time	Area	Area%
Total			

PDA Ch1 254nm

Peak#	Ret. Time	Area	Area%
1	5.805	8478135	100.000
Total		8478135	100.000

Figure S27: 4-Nitrobenzaldehyde **7** determined by HPLC with kromasil column (hexane : 2-propanol = 90 : 10) ; flow rate 1 ml/min; PDA 254 nm; retention time: = 5.81 min.

SHIMADZU LabSolutions **Analysis Report**

<Sample Information>

Sample Name	: ZAR_415_workup_kromasil_90_10_1.0		
Sample ID	: ZAR_415_workup_kromasil_90_10_1		
Data Filename	: ZAR_415_workup_kromasil_90_10_1.0.lcd		
Method Filename	: GRA-140_ODH_98_2_1.0.lcm		
Batch Filename	:		
Vial #	: 1-83	Sample Type	: Unknown
Injection Volume	: 15 uL		
Date Acquired	: 16.01.2024 12:30:23	Acquired by	: System Administrator
Date Processed	: 16.01.2024 13:17:59	Processed by	: System Administrator

<Chromatogram>

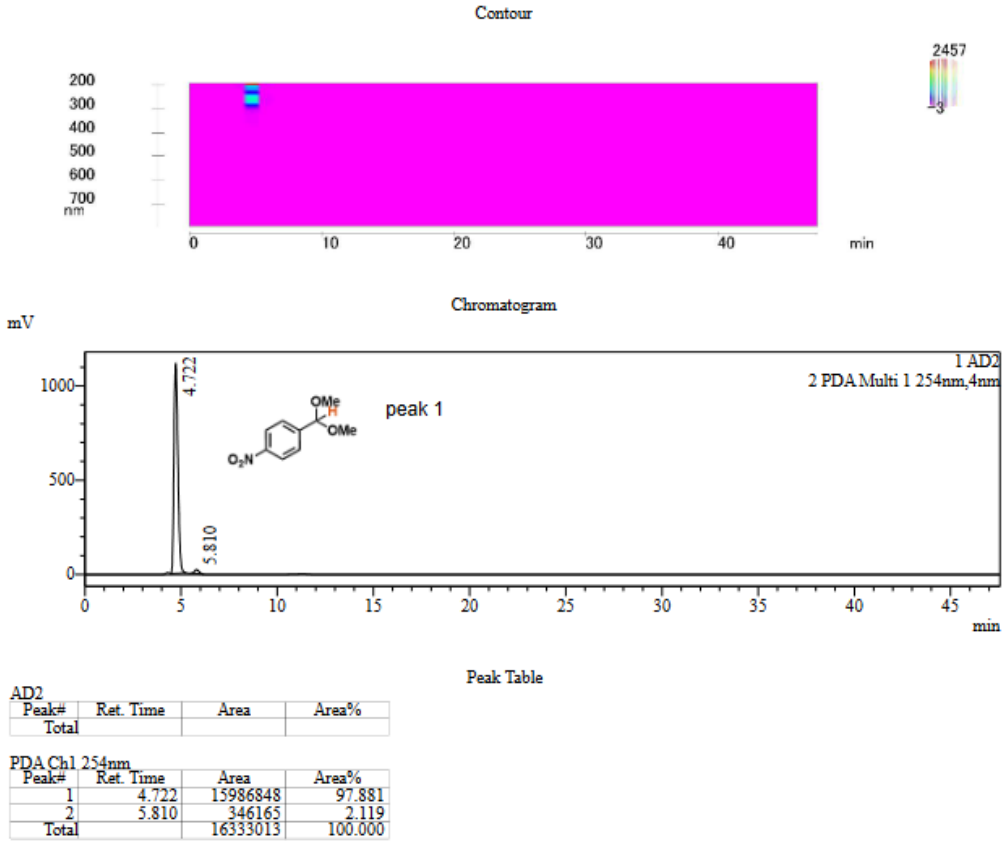

Peak Table

AD2

Peak#	Ret. Time	Area	Area%
Total			

PDA Ch1 254nm

Peak#	Ret. Time	Area	Area%
1	4.722	15986848	97.881
2	5.810	346165	2.119
Total		16333013	100.000

Figure S28: Acetal **10** determined by HPLC with kromasil column (hexane : 2-propanol = 90 : 10) ; flow rate 1 ml/min; PDA 254 nm; retention time: = 4.72 min.

SHIMADZU LabSolutions **Analysis Report**

<Sample Information>

Sample Name	: ZAR-275_kromasil_90_10_1.0		
Sample ID	: ZAR-275_kromasil_90_10_1.0		
Data Filename	: ZAR-275_kromasil_90_10_1.0.lcd		
Method Filename	: GRA-140_ODH_98_2_1.0.lcm		
Batch Filename	:		
Vial #	: 1-76	Sample Type	: Unknown
Injection Volume	: 15 uL		
Date Acquired	: 16.01.2024 10:26:18	Acquired by	: System Administrator
Date Processed	: 16.01.2024 10:46:21	Processed by	: System Administrator

<Chromatogram>

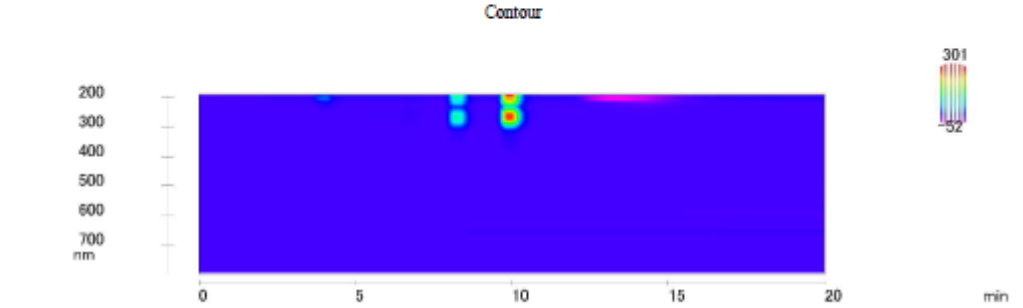

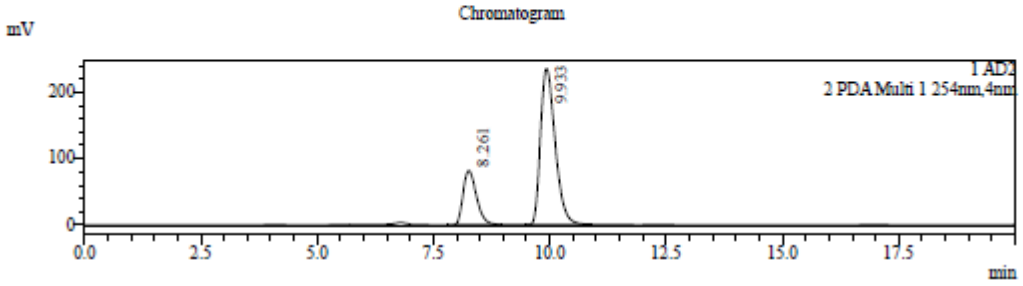

AD2

Peak#	Ret. Time	Area	Area%
Total			

PDA Ch1 254nm

Peak#	Ret. Time	Area	Area%
1	8.261	1625945	24.032
2	9.933	5139938	75.968
Total		6765883	100.000

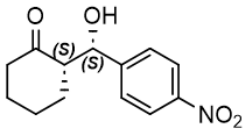

syn-**9**

t_R = 8.26 min.

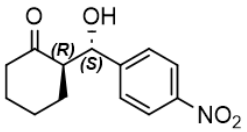

anti-**9**

t_R = 9.93 min.

Figure S29: Diastereomeric ratio of *syn*-**9** and *anti*-**9** determined by achiral HPLC with kromasil column (hexane : 2-propanol = 90 : 10) ; flow rate 1 ml/min; PDA 254 nm; retention time: *syn*-***9*** diastereomer = 8.26 min, *anti*-**9** diastereomer = 9.93 min.

SHIMADZU LabSolutions **Analysis Report**

<Sample Information>

Sample Name	: ZAR-275.2		
Sample ID	: ZAR-275.2_ADH_90_10_0.8		
Data Filename	: ZAR-275.2_ADH_90_10_0_verd.lcd		
Method Filename	: Kirchhof_EnIN_Tosyl.lcm		
Batch Filename	:		
Vial #	: 1-76	Sample Type	: Unknown
Injection Volume	: 10 uL		
Date Acquired	: 13.06.2023 11:53:27	Acquired by	: System Administrator
Date Processed	: 13.06.2023 12:51:43	Processed by	: System Administrator

<Chromatogram>

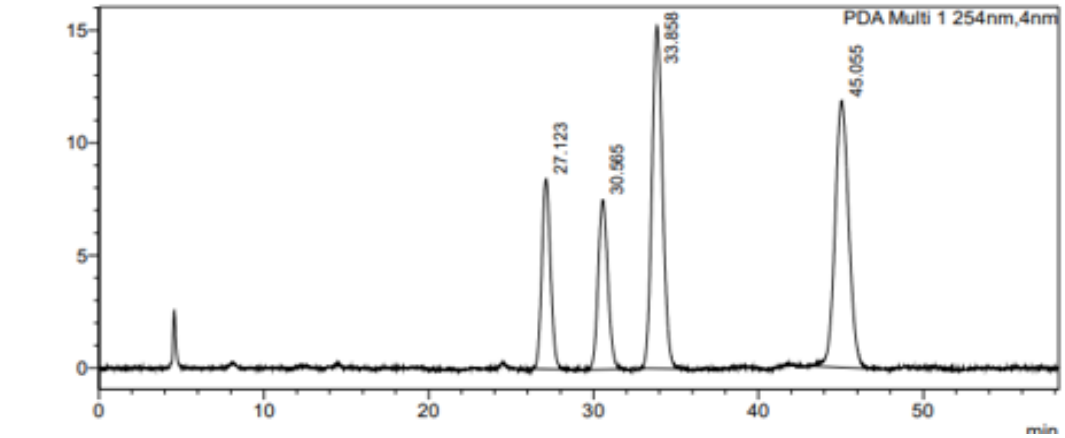

<Peak Table>

AD2

Peak#	Ret. Time	Area	Area%
Total			

PDA Ch1 254nm

Peak#	Ret. Time	Area	Area%
1	27.123	309168	15.590
2	30.565	309270	15.595
3	33.858	678834	34.231
4	45.055	685806	34.583
Total		1983078	100.000

Peak Table

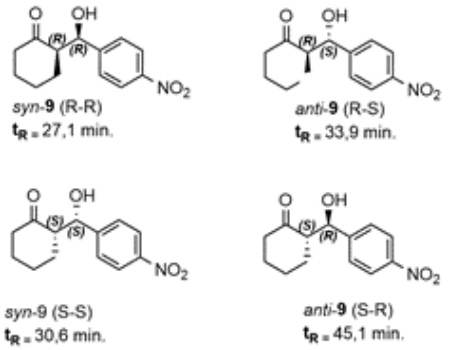

Figure S30: Enantiomeric excess of aldol **9** determined by HPLC with CHIRALPAK AD-H column using the prepared racemic standard, 250 x 4.6 mm, 5 µm , (hexane : 2-propanol = 90 : 10) ; flow rate 0.8 ml/min; PDA 254 nm; retention time: minor diastereomer: 27.1 min (major), 30.6 min (minor); major diastereomer: 33.8 min (major), 45.1 min (minor).

8. NMR spectra

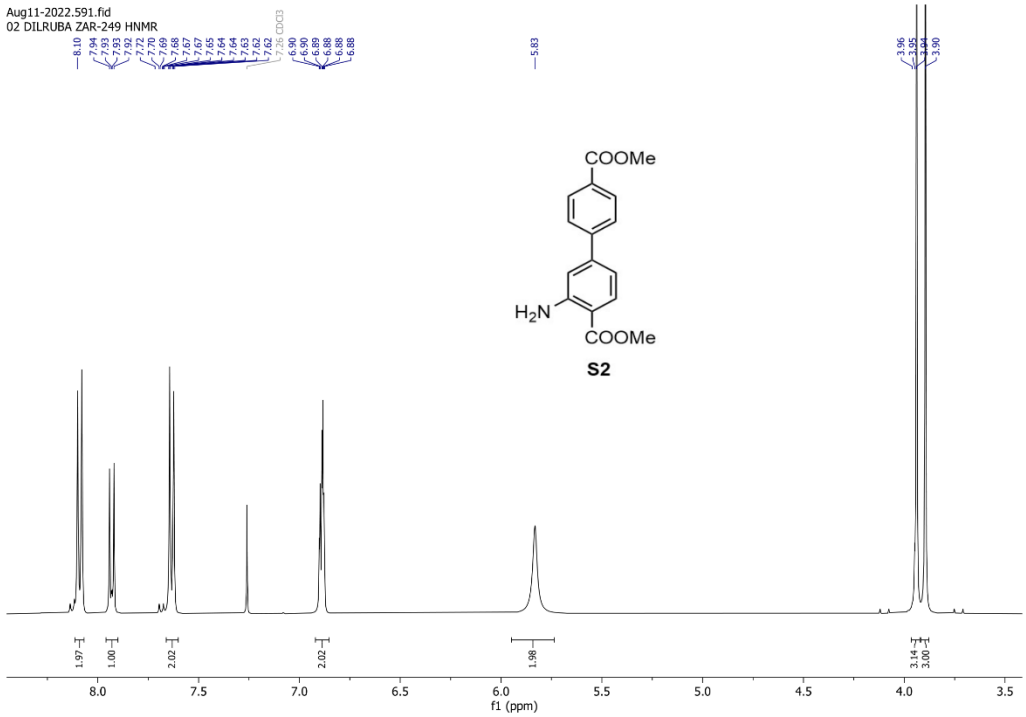

Figure S31: ^{1}H NMR spectrum (400 MHz, $CDCl_3$) of **S2.**

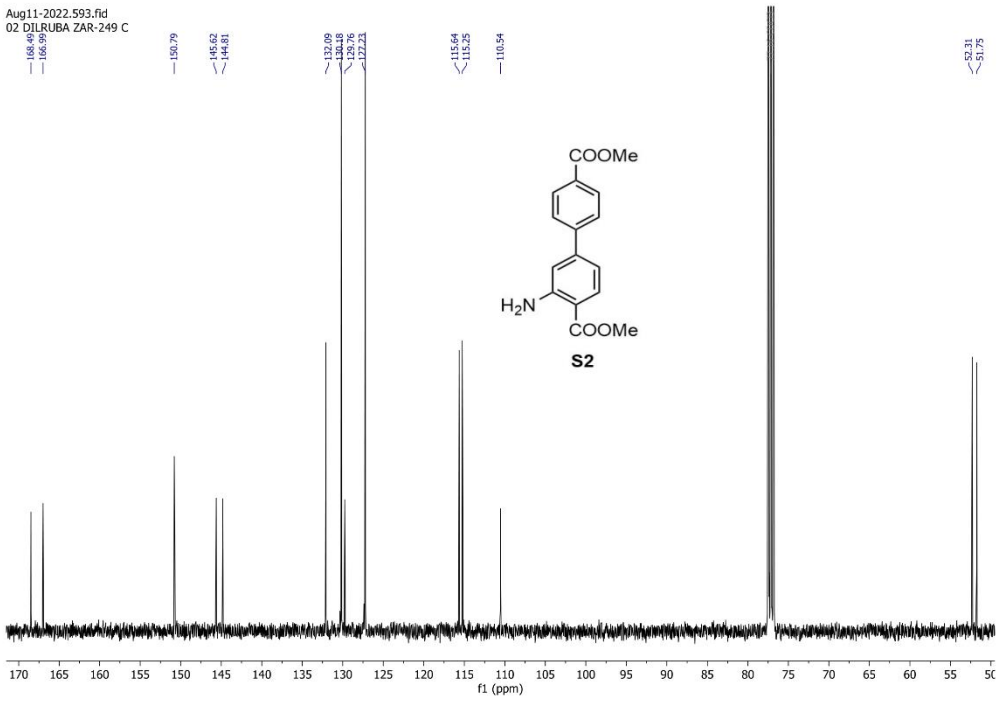

Figure S32: ^{13}C NMR spectrum (101 MHz, $CDCl_3$) of **S2.**

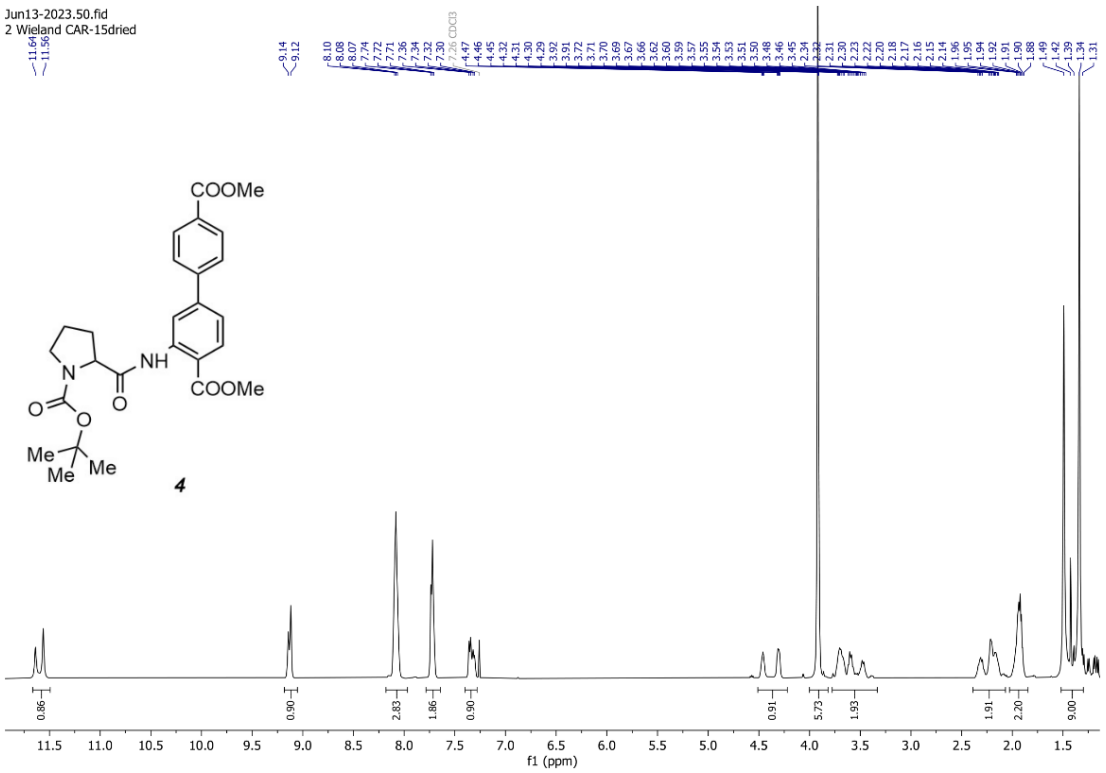

Figure S33: ^{1}H NMR spectrum (400 MHz, $CDCl_3$) of **4**.

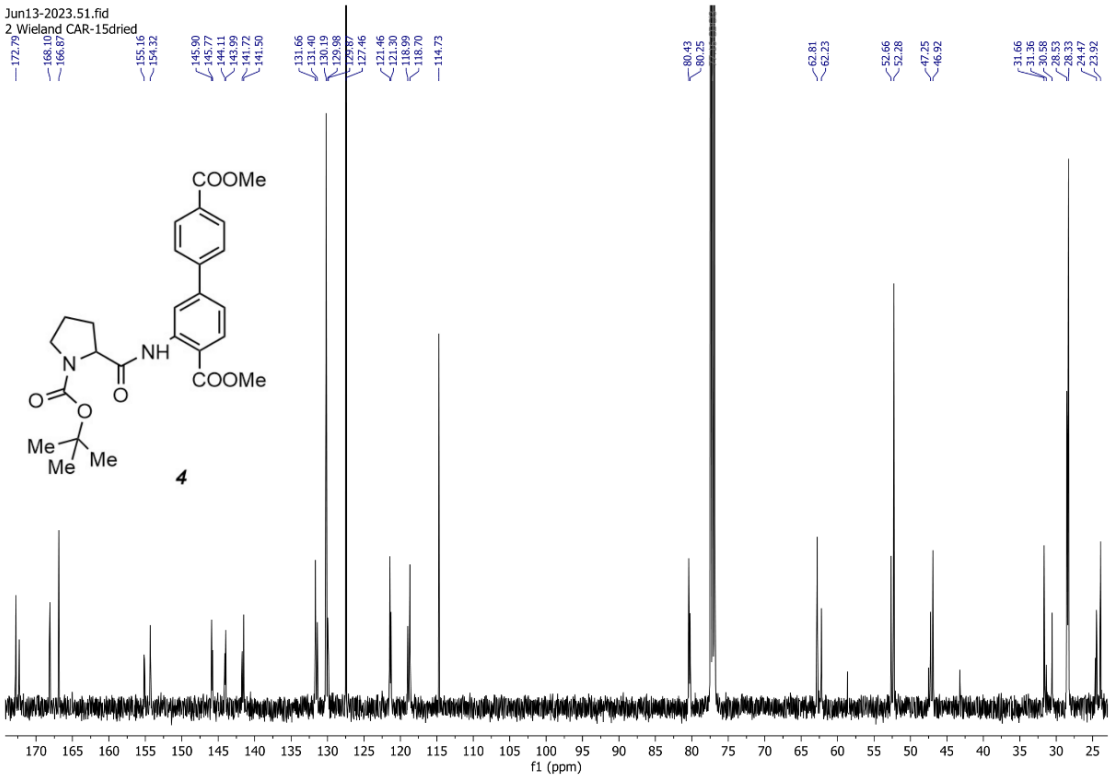

Figure S34: ^{13}C NMR spectrum (126 MHz, $CDCl_3$) of **4**.

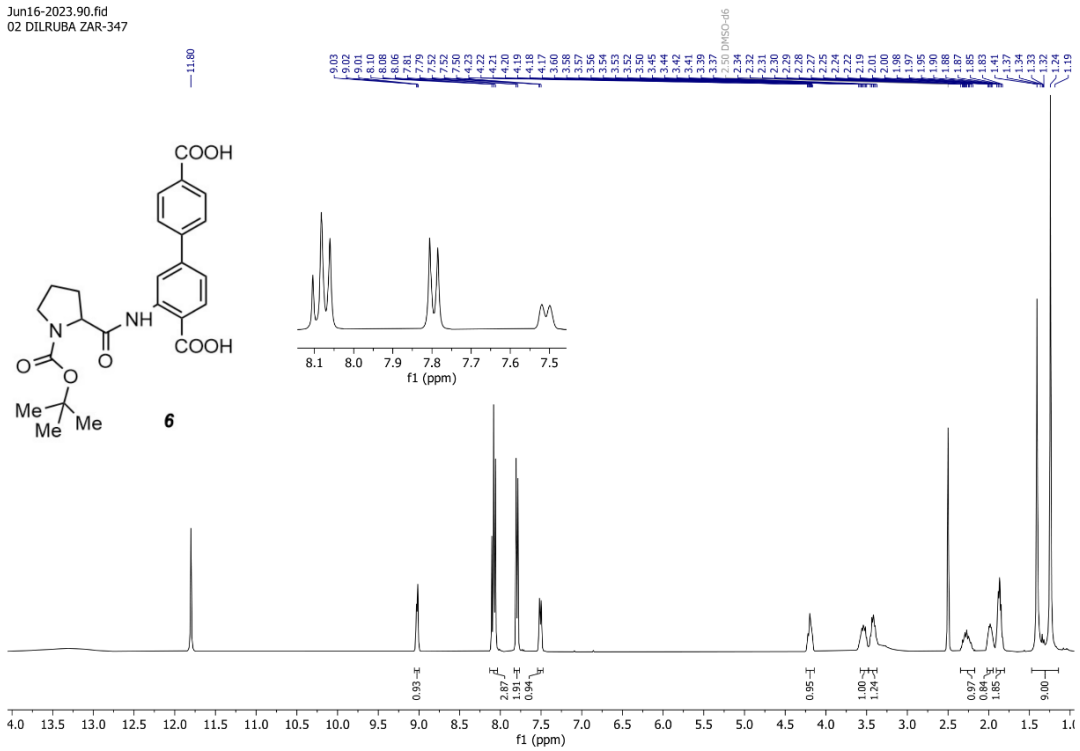

Figure S35: ^{1}H NMR spectrum (400 MHz, DMSO-d_6) of **6**.

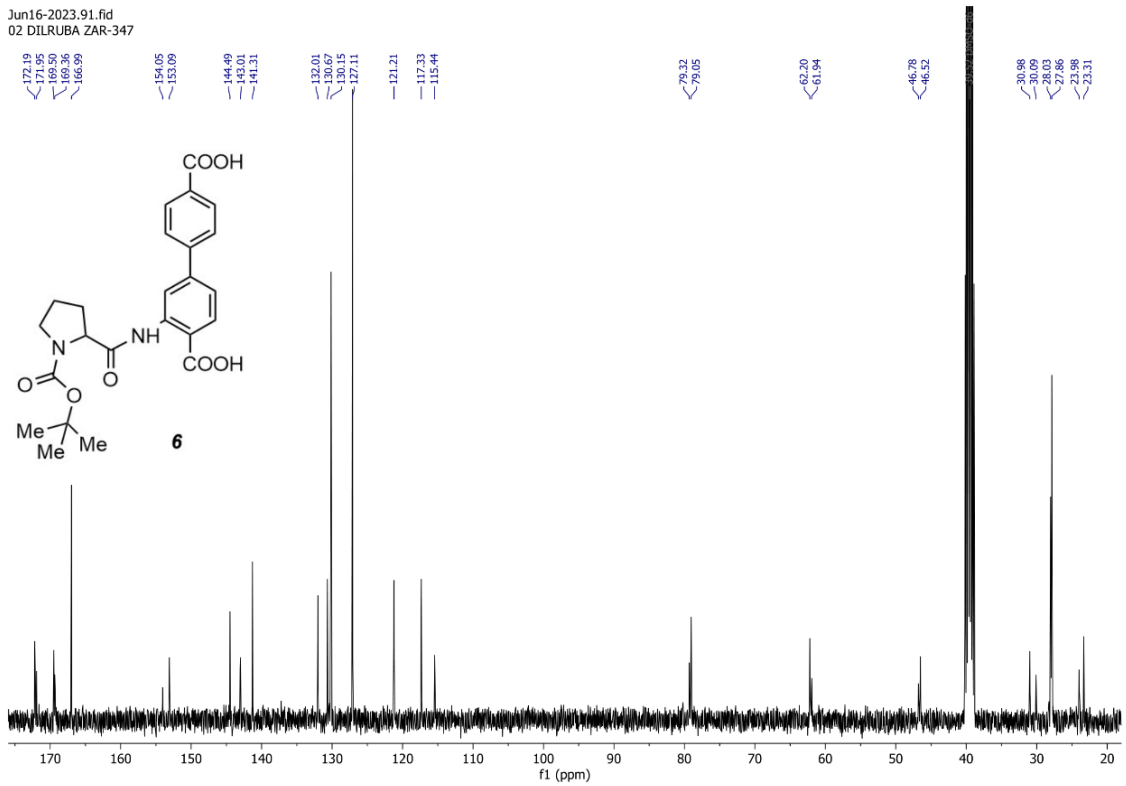

Figure S36: ^{13}C NMR spectrum (101 MHz, DMSO-d_6) of **6**.

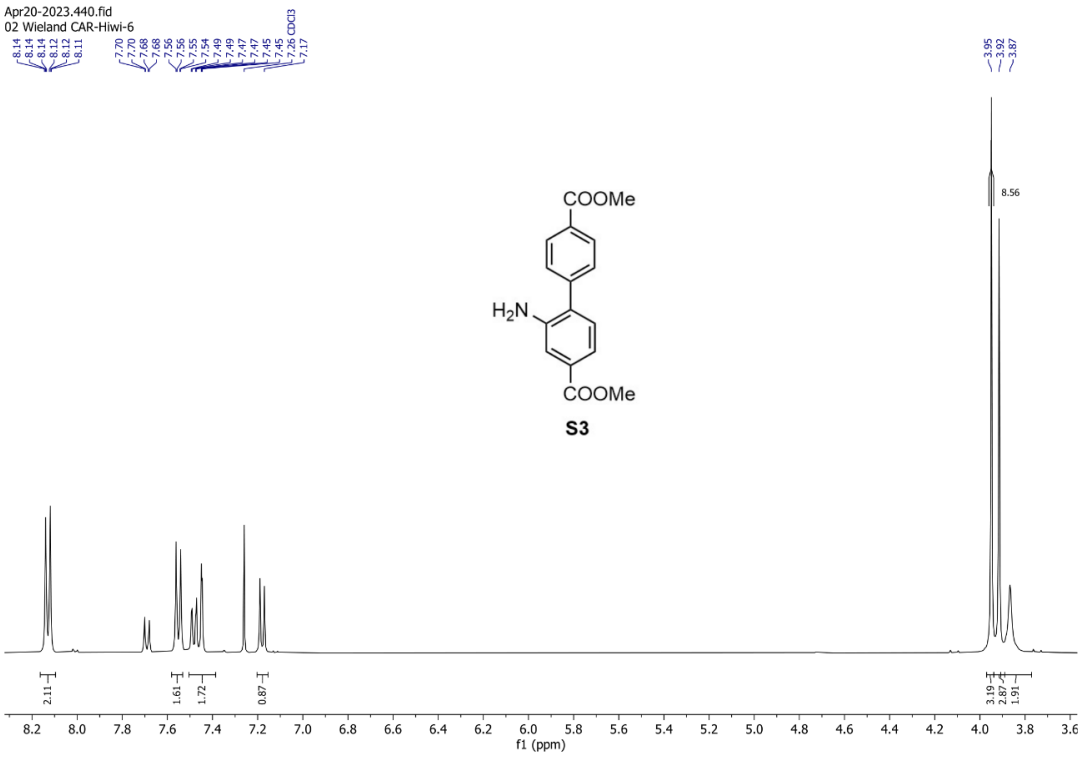

Figure S37: ^{1}H NMR spectrum (400 MHz, $CDCl_3$) of **S3**.

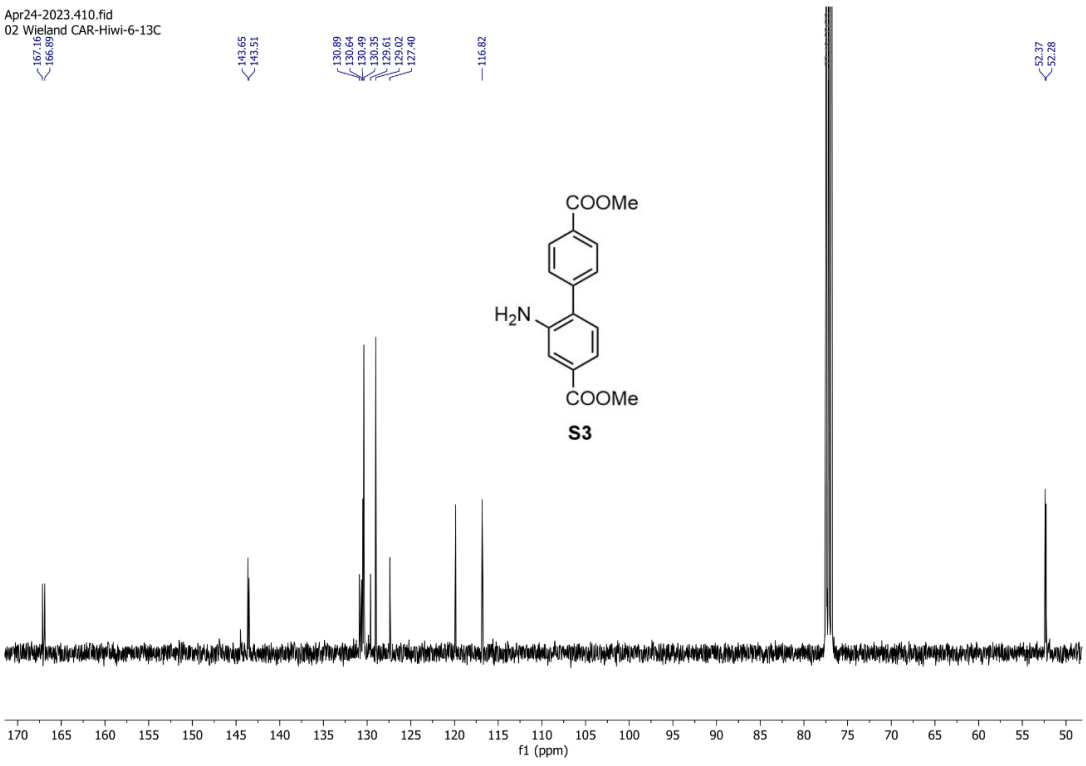

Figure S38: ^{13}C NMR spectrum (101 MHz, $CDCl_3$) of **S3**.

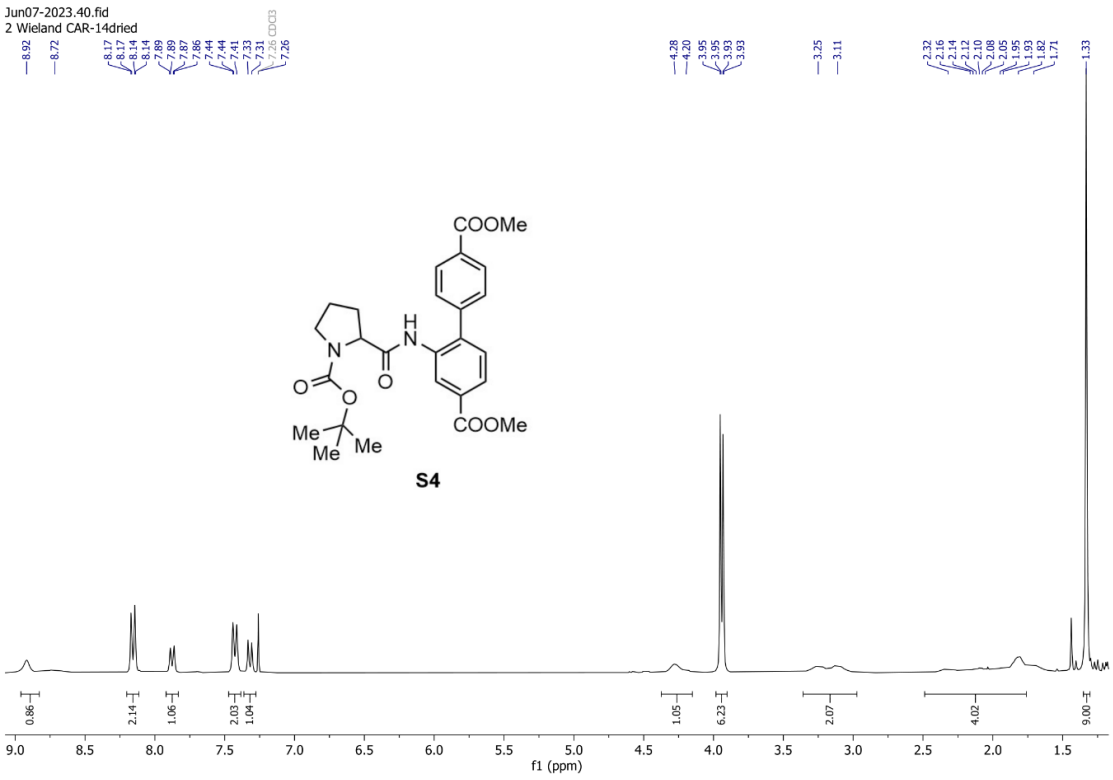

Figure S39: ^{1}H NMR spectrum (300 MHz, $CDCl_3$) of **S4**.

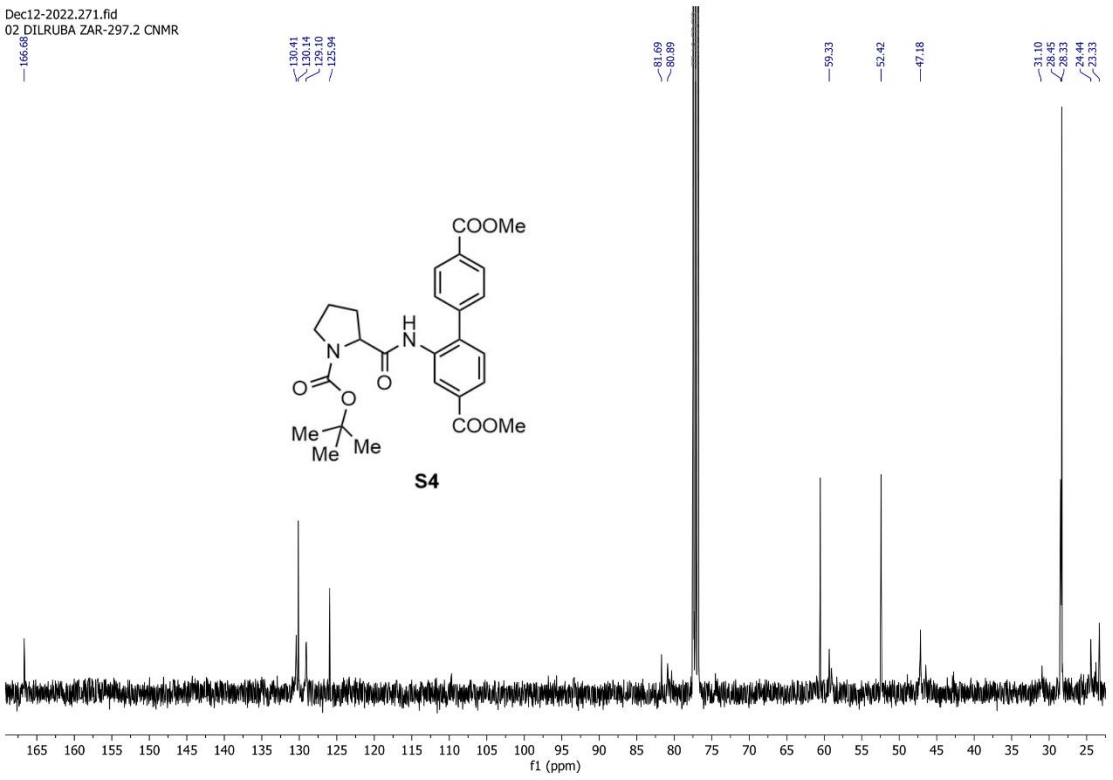

Figure S40:^{13}C NMR spectrum (101 MHz, $CDCl_3$) of **S4**.

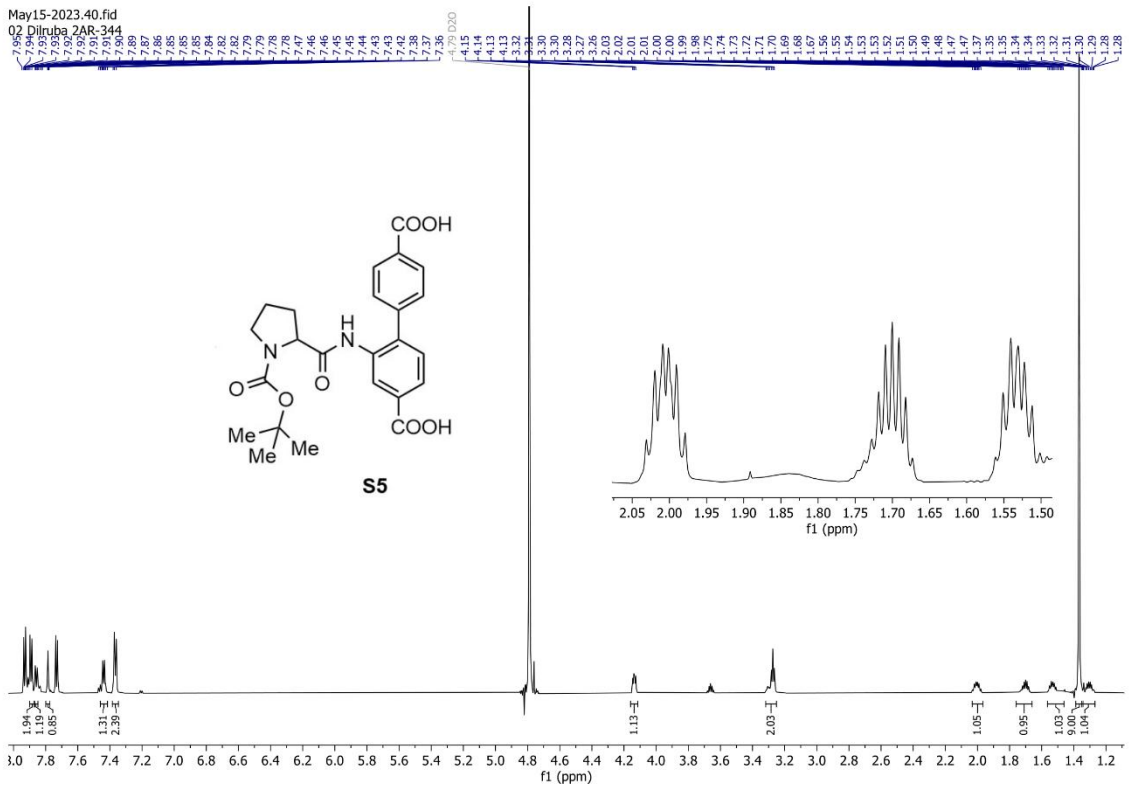

Figure S41: ^{1}H NMR spectrum (700 MHz, D_2O/KOH) of **S5**.

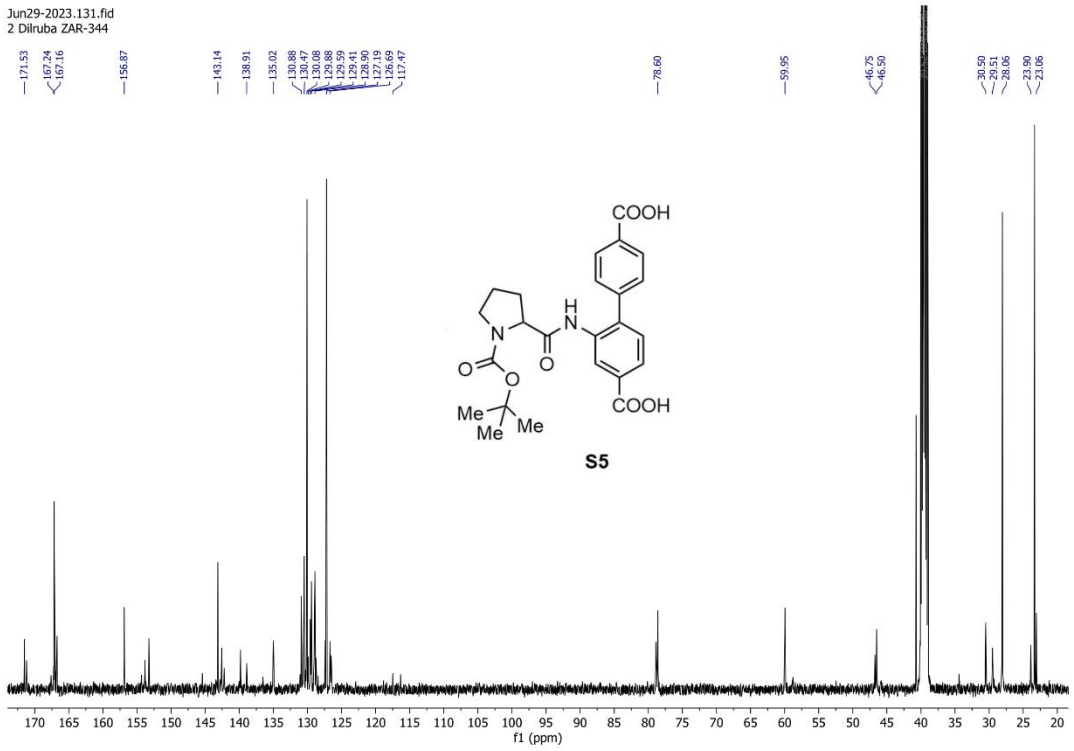

Figure S42:^{13}C NMR spectrum (126 MHz, DMSO-d_6) of **S5**.

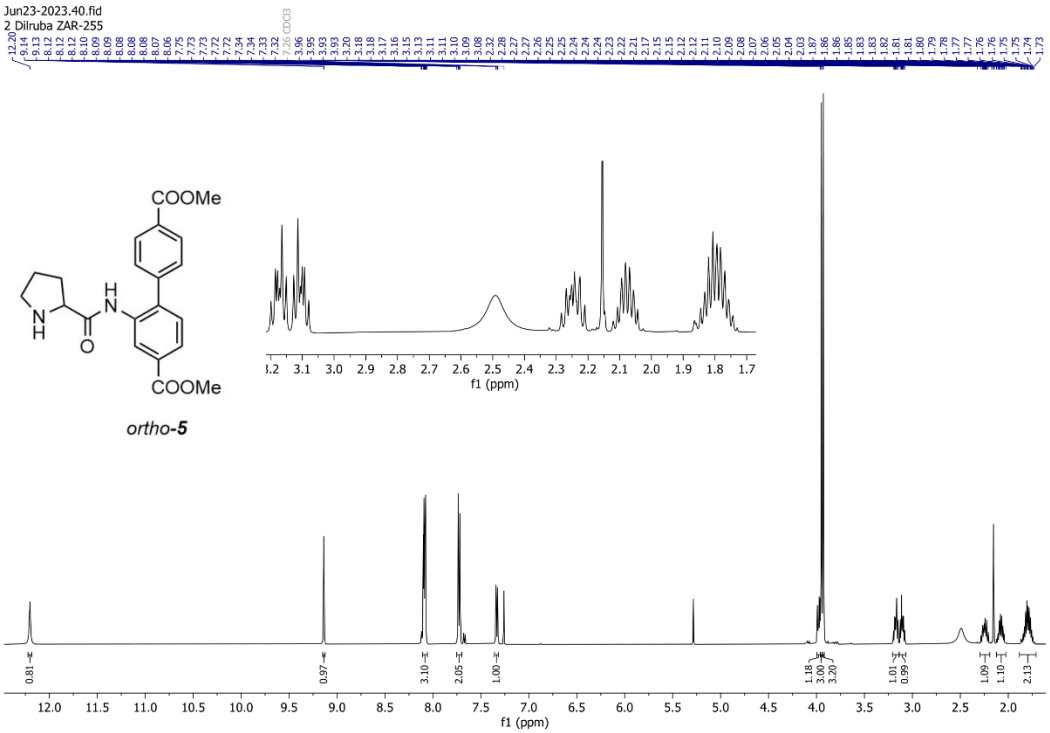

Figure S43: ^{1}H NMR spectrum (500 MHz, $CDCl_3$) of *ortho*-**5.**

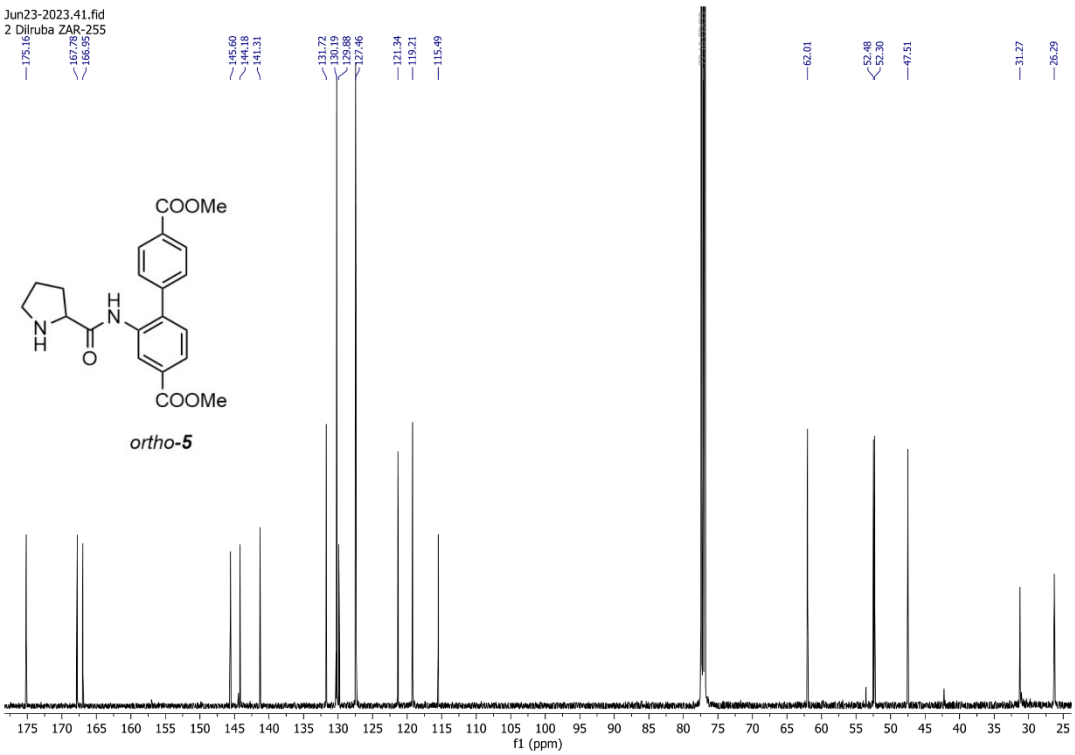

Figure S44: ^{13}C NMR spectrum (126 MHz, $CDCl_3$) of *ortho*-**5.**

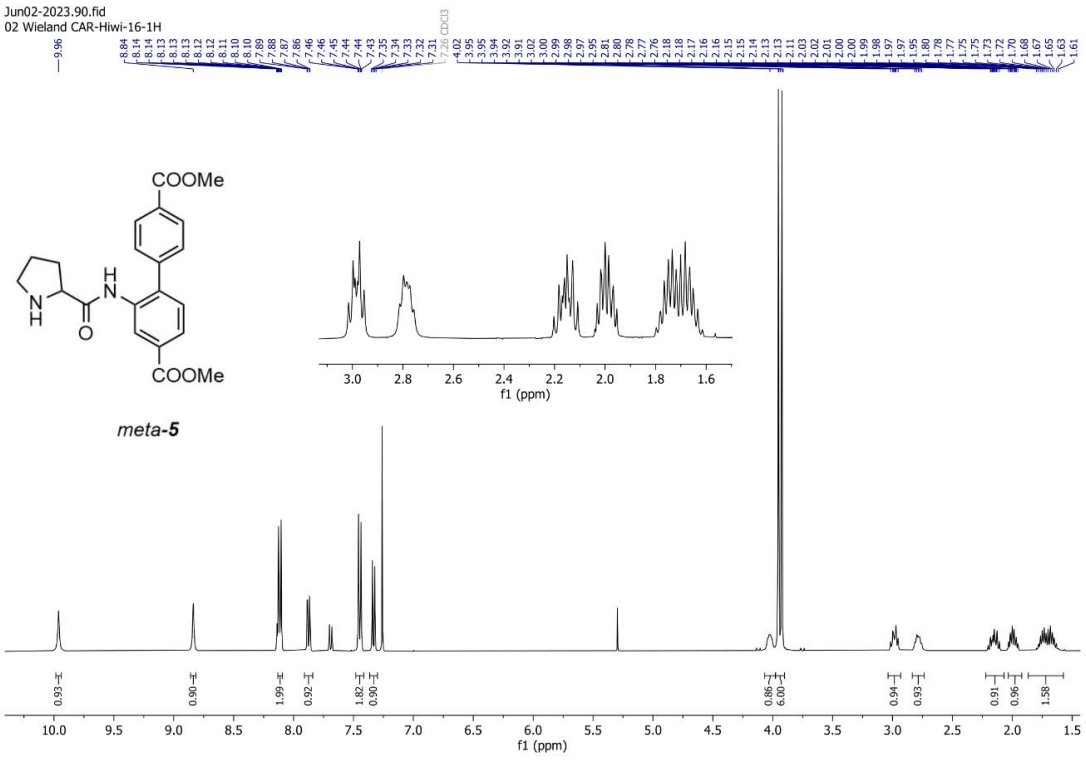

Figure S45: ^{1}H NMR spectrum (400 MHz, $CDCl_3$) of *meta*-**5.**

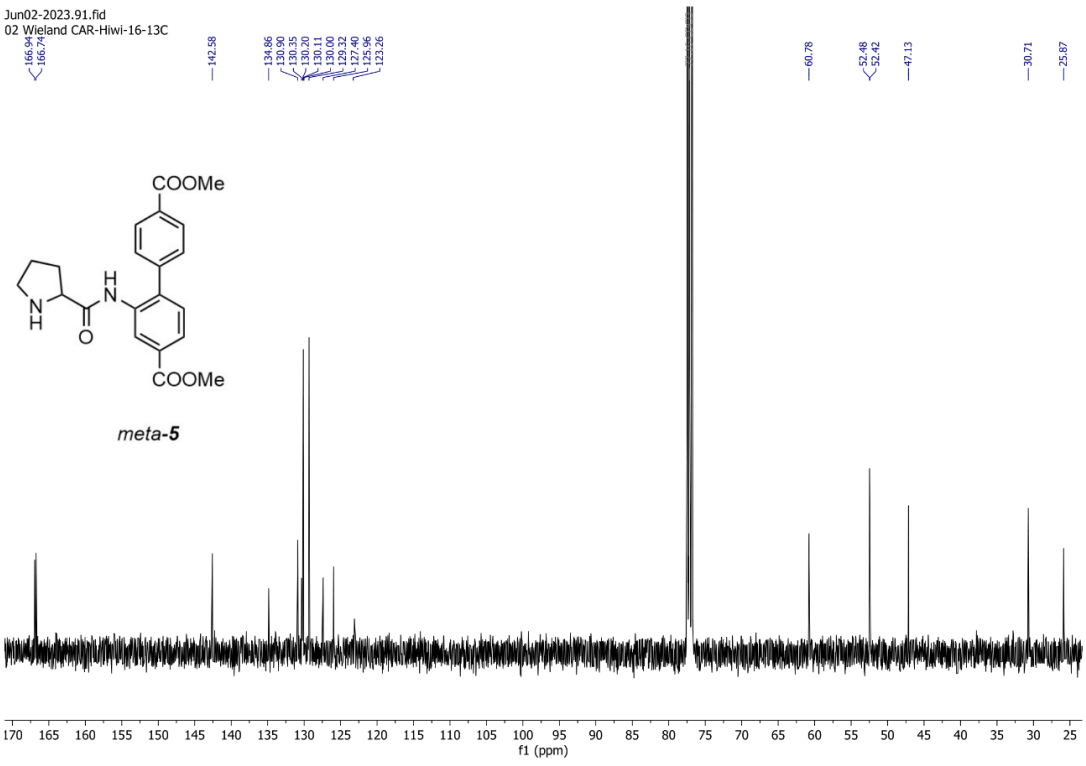

Figure S46: ^{13}C NMR spectrum (101 MHz, $CDCl_3$) of *meta*-**5.**

9. Supplementary references

1 O. M. Yaghi, M. O'Keeffe, N. W. Ockwig, H. K. Chae, M. Eddaoudi, J. Kim, Reticular synthesis and the design of new materials, *Nature,* 2003, **423**, 705-714.

2 H.-C. Zhou, J. R. Long, O. M. Yaghi*, Introduction to Metal–Organic Frameworks,* ACS Publications, 2012, **112***,* 673-674.

3 Z. Wang, S. M. Cohen, Postsynthetic modification of metal–organic frameworks, *Chem. Soc. Rev.,* 2009, **38**, 1315-1329.

4 B. I. Ahmad, K. T. Keasler, E. E. Stacy, S. Meng, T. J. Hicks, P. J. Milner, MO0Fganic Chemistry: Challenges and Opportunities for Metal–Organic Frameworks in Synthetic Organic Chemistry, *Chem. Mater.,* 2023, **35**, 4883-4896.

5 Q. Wang, D. Astruc, State of the art and prospects in metal–organic framework (MOF)-based and MOF-derived nanocatalysis *Chem. Rev.,* 2019, **120**, 1438-1511.

6 S. G. Balasubramani, G. P. Chen, S. Coriani, M. Diedenhofen, M. S. Frank, Y. J. Franzke, F. Furche, R. Grotjahn, M. E. Harding, C. Hättig, TURBOMOLE: Modular program suite for ab initio quantum-chemical and condensed-matter simulations, *J. Chem. Phys.,* 2020, **152**, 184107.

7 P. Sherwood, A. H. de Vries, M. F. Guest, G. Schreckenbach, C. R. A. Catlow, S. A. French, A. A. Sokol, S. T. Bromley, W. Thiel, A. J. Turner, QUASI: A general purpose implementation of the QM/MM approach and its application to problems in catalysis, *J. Mol. Struct.,* 2003, **632**, 1-28.

8 S. Metz, J. Kästner, A. A. Sokol, T. W. Keal, P. Sherwood, ChemShell—a modular software package for QM/MM simulations, *Wiley Interdisciplinary Reviews: Comput. Mol. Sci.,* **2014**, *4*, 101-110.

9 J. Kästner, J. M. Carr, T. W. Keal, W. Thiel, A. Wander, P. Sherwood, DL-FIND: An Open-Source Geometry Optimizer for Atomistic Simulations, *J. Phys. Chem. A.,* 2009, **113**, 11856-11865.

10 S. Øien, D. Wragg, H. Reinsch, S. Svelle, S. Bordiga, C. Lamberti, K. P. Lillerud, Detailed structure analysis of atomic positions and defects in zirconium metal–organic frameworks, *Cryst. Growth Des.*, 2014, **14**, 5370-5372.

11 M. J. Abraham, T. Murtola, R. Schulz, S. Páll, J. C. Smith, B. Hess, E. Lindahl, GROMACS: High performance molecular simulations through multi-level parallelism from laptops to supercomputers, *SoftwareX,* 2015, **1**, 19-25.

12 a) S. Jo, T. Kim, V. G. Iyer, W. Im, CHARMM-GUI: a web-based graphical user interface for CHARMM, *J. Comput. Chem.,* 2008, **29**, 1859-1865; b) B. R. Brooks, C. L. Brooks III, A. D. Mackerell Jr, L. Nilsson, R. J. Petrella, B. Roux, Y. Won, G. Archontis, C. Bartels, S. Boresch, CHARMM: The Biomolecular Simulation Program, *J. Comput. Chem.,* 2009, **30**, 1545-1614.

13 J. Lee, X. Cheng, J. M. Swails, M. S. Yeo, P.K. Eastman, J. A.Lemkul, S. Wei, J. Buckner, J. C. Jeong, Y. Qi, S. Jo, *"CL 3rd Brooks, AD J. MacKerell, JB Klauda, W. Im, CHARMM-GUI input generator for NAMD, GROMACS, AMBER, OpenMM, and CHARMM/OpenMM simulations using the CHARMM36 additive force field, J. Chem. Theor. Comput., 2016,* **12***, 405-413.*

14 (a) N. Ko, J. Hong, S. Sung, K. E. Cordova, H. J. Park, J. K., Yang, J. Kim, A significant enhancement of water vapour uptake at low pressure by amine-functionalization of UiO-67. *Dalton Trans.*, 2015, **44**, 2047-2051; (b) T. F. Willems, C. H. Rycroft, M. Kazi, J. C. Meza, M. Haranczyk, Algorithms and tools for high-throughput geometry-based analysis of crystalline porous materials, *Micropor. Mesopor. Mat.,* 2012, **149**, 134-141.

15 C. Kutzscher, G. Nickerl, I. Senkovska, V. Bon, S. Kaskel, Proline functionalized UiO-67 and UiO-68 type metal–organic frameworks showing reversed diastereoselectivity in aldol addition reactions, *Chem. Mater.,* 2016, **28**, 2573-2580.

16 H. J. Berendsen, J. v. Postma, W. F. Van Gunsteren, A. DiNola, J. R. Haak, Molecular dynamics with coupling to an external bath, *J. Chem. Phys.,* 1984, **81**, 3684-3690.

17 T. Darden, D. York, L. Pedersen, Particle mesh Ewald: An N·log(N) method for Ewald sums in large systems, *J. Chem. Phys.,* 1993, **98**, 10089-10092.

18 S. Páll, B. Hess, A flexible algorithm for calculating pair interactions on SIMD architectures, *Comput. Phys. Commun.,* 2013, **184**, 2641-2650.

19 B. Hess, P-LINCS: A parallel linear constraint solver for molecular simulation, *J. Chem. Theory Comput.,* 2008, **4**, 116-122.

20 J. D. Hunter, Matplotlib: A 2D graphics environment, *Comput. Sci. Eng.,* **2007**, **9**, 90-95.

21 L. Liu, T.-Y. Zhou, S. G. Telfer, Modulating the performance of an asymmetric organocatalyst by tuning its spatial environment in a metal–organic framework, *JACS,* 2017, **139**, 13936-13943.

22 C. Kutzscher, H. C. Hoffmann, S. Krause, U. Stoeck, I. Senkovska, E. Brunner, S. Kaskel, Proline functionalization of the mesoporous metal− organic framework DUT-32, *Inorg. Chem.,* 2015, **54**, 1003-1009.

23 D. J. Lun, G. I. Waterhouse, S. G. Telfer, A general thermolabile protecting group strategy for organocatalytic metal− organic frameworks, *JACS***,** 2011, **133**, 5806-5809.

24 K. D. Nguyen, C. Kutzscher, S. Ehrling, I. Senkovska, V. Bon, M. de Oliveira Jr, T. Gutmann, G. Buntkowsky, S. Kaskel, Insights into the role of zirconium in proline functionalized metal-organic frameworks attaining high enantio-and diastereoselectivity, *J. Catal.,* 2019, **377**, 41-50.

25 Z. Gong, C. Wei, Y. Shi, Q. Zheng, Z. Song, Z. Liu, Novel chiral bifunctional l-thiazoline-amide derivatives: Design and application in the direct enantioselective aldol reactions, *Tetrahedron,* 2014, **70**, 1827-1835.

26 T. Kawajiri, M. Kato, H. Nakata, R. Goto, S.-y. Aibara, R. Ohta, H. Fujioka, H. Sajiki, Y. Sawama, Synthesis of 1, 2-Dihydroisoquinolines by a Modified Pomeranz–Fritsch Cyclization, *JOC.,* 2019, **84**, 3853-3870.

27 J. Paradowska, M. Pasternak, B. Gut, B. Gryzło, J. Mlynarski, Direct Asymmetric Aldol Reactions Inspired by Two Types of NaturalAldolases: Water-Compatible Organocatalysts and ZnII Complexes, *JOC.*, 2012, **77**, 173 - 187.

28 B. List, Proline-Catalyzed Asymmetric Reactions, *Tetrahedron,* 2002, **58**, 5578 – 5590.

29 L.-J. Yu, M. T. Blyth, M. L. Coote, Re-Examination of Proline-Catalyzed Intermolecular Aldol Reactions: An Ab Initio Kinetic Modelling Study, *Top. Catal.,* 2022, **65**, 354 – 365.

30 T. M. Bräuer, Q. Zhang, K. Tiefenbacher, Iminium catalysis inside a self-assembled supramolecular capsule: scope and mechanistic studies; *J. Am. Chem. Soc.,* 2017, **139**, 17500 – 17507.

31 G. C. Shearer, S. Chavan, S. Bordiga, S. Svelle, U. Olsbye, K. P. Lillerud, Defect engineering: tuning the porosity and composition of the metal–organic framework UiO-66 via modulated synthesis, *Chem. Mat.,* 2016, **28**, 3749-3761.

32 D. K. Sannes, S. Øien-Ødegaard, E. Aunan, A. Nova U. Olsbye, Quantification of linker defects in UiO-type metal–organic frameworks. *Chem. Mat.,* 2023,**35**, 3793-3800.